Hindawi
Geofluids
Volume 2021, Article ID 6629758, 20 pages
https://doi.org/10.1155/2021/6629758

Research Article

A Study on the Heterogeneity Characteristics of Geological Controls on Coalbed Methane Accumulation in Gujiao Coalbed Methane Field, Xishan Coalfield, China

Taotao Yan,[1,2] **Shan He**,[3] **Yadong Bai**,[4] **Zhiyong He**,[5] **Dameng Liu**,[2] **Fangui Zeng**,[1] **Xiaozhen Chen**,[1] **and Xinyu Fu**[1]

[1]*Department of Earth Science and Engineering, Taiyuan University of Technology, Taiyuan, 030024 Shanxi, China*
[2]*Coal Reservoir Laboratory of National Engineering Research Center of CBM Development & Utilization, China University of Geosciences, Beijing 100083, China*
[3]*Shanxi CBM Exploration and Development Branch, PetroChina Huabei Oilfield Company, Shanxi 048000, China*
[4]*Research Institute of Petroleum Exploration and Development-Northwest, Petrochina, Lanzhou 730000, China*
[5]*Exploration Company, Sinopec, Chengdu 610041, China*

Correspondence should be addressed to Taotao Yan; taotao87225@163.com

Received 31 December 2020; Revised 31 January 2021; Accepted 16 February 2021; Published 13 March 2021

Academic Editor: Yingfang Zhou

Commercial exploration and exploitation of coalbed methane (CBM) in Gujiao coalbed methane (CBM) field, Xishan coalfield, have rapidly increased in recent decades. The Gujiao CBM field has shown strong gas distribution heterogeneity, low gas content, and wide distribution of wells with low production. To better understand the geological controlling mechanism on gas distribution heterogeneity, the coal reservoir evolution history and CBM accumulation process have been studied on the base of numerical simulation work. The burial history of coal reservoir can be classified into six stages: shallowly buried stage; deeply buried stage; uplifting stage; short-term tectonic subsidence stage; large-scale uplifting stage; and sustaining uplifting and structural inversion stage. Mostly, coal seams have experienced two-time thermal metamorphisms with twice hydrocarbon-generation processes in this area, whereas in the southwest part, the coal seams in there suffered three-time thermal metamorphisms and hydrocarbon-generation processes. The critical tectonic events of the Indosinian, Yanshanian, and Himalayan orogenies affect different stages of the CBM reservoir accumulation evolution process. The Indosinian orogeny mainly controls the primary CBM generation. The Yanshanian orogeny dominates the second and third gas generation and migration processes. The Himalayan orogeny mainly affects the gas dissipation process and current CBM distribution heterogeneity.

1. Introduction

As a clean and unconventional natural gas resource, coalbed methane (CBM) is considered to be the most potential source of energy with broad prospects for commercial development. In recent years, the exploitation of CBM in coal-bearing basins has achieved tremendous success in China, especially in Qinshui Basin and Ordos Basin [1–9]. The exploration and exploitation of CBM in Xishan coalfield start relatively late, and the research bases of CBM geology are poor in there. Previous research works show that the geological background of Xishan coalfield is very unique. The coalfield had experienced multistage tectonic deformation accompanied with complex structural morphology [10, 11]. The maturity of the Pennsylvanian and Permian coal seams in Xishan coalfield shows strong heterogeneity and ranges from high-volatile bituminous A to anthracite [12]. Gujiao CBM field is one of the most important areas for the exploration and exploitation of CBM in Xishan coalfield. The proved CBM resource in this area is about 82.9 billion m^3, showing strongly economic developmental potential [13]. Since 2011, more than 700 CBM wells have been drilled in this

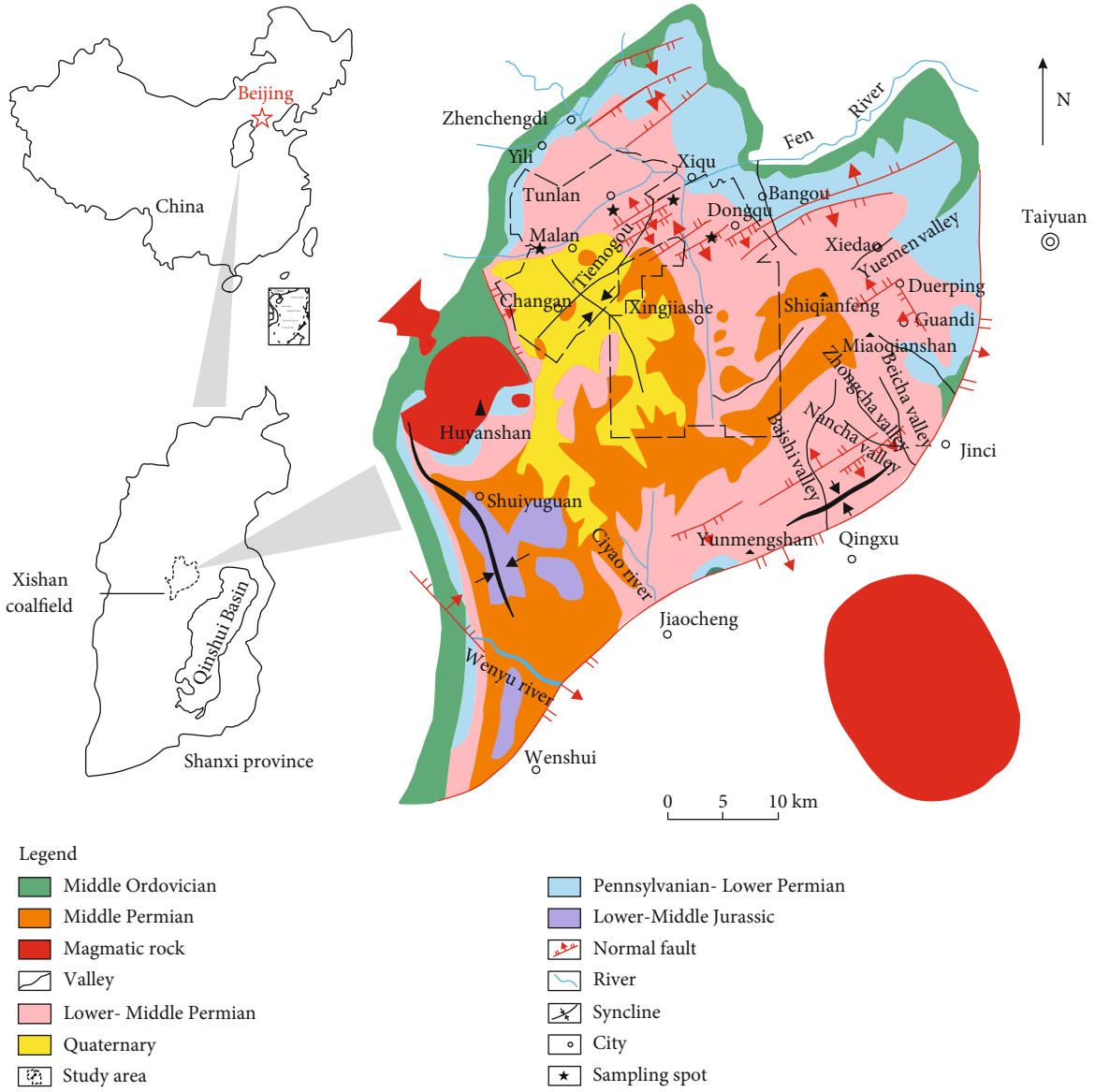

Figure 1: Location of the study area and structural outline of Xishan coalfield.

area. However, the exploitation performance of these CBM wells is not very well. The average of daily gas production is only about 277 m^3 [14]. Bian et al. proposed that the complicated structural character of coal reservoir and the ambiguity of resource evaluation process are the main reasons for this poor gas production phenomenon [15].

In recent years, many research works have been carried out in Gujiao CBM field, including geological structural character analysis [16], sedimentary environment restoration [17–24], coal reservoir energy field dissection [25–28], coal reservoir physical property characterization [29, 30], favorable area evaluation [16, 25, 31–33], and qualitative research on CBM accumulation [12, 34–44]. However, to the best of the authors' knowledge, effective research on the coal reservoir evolution and CBM accumulation process has not been conducted in Gujiao CBM field.

The coal reservoir evolution process is a complex dynamic process which includes coal organic matter maturation, gas generation, sorption, migration, diffusion, pooling, and accumulation processes [45]. These dynamic processes were mainly controlled by the evolution characteristics (tectonic subsidence history, geothermal and paleotectonic stress field evolution history) of coal bearing basin [45]. Basin-scale investigations of the CBM reservoir evolution process have been performed in the United States [46, 47], Australia [48, 49], Russia [50], Belgium [51], Ukraine [52], and China [45, 53, 54].

In this study, the method proposed in our previous work [45] was used to study this complex dynamic process in Gujiao CBM field. The evolution histories of sedimentary-burial process, thermal field, and hydrocarbon generation in CBM reservoir were simulated by analyzing the geophysical logging data. Then, a dynamic equilibrium model was utilized to explain the evolution of CBM reservoir. Finally, the controlling mechanism of four critical tectonic events on CBM accumulation heterogeneity was investigated.

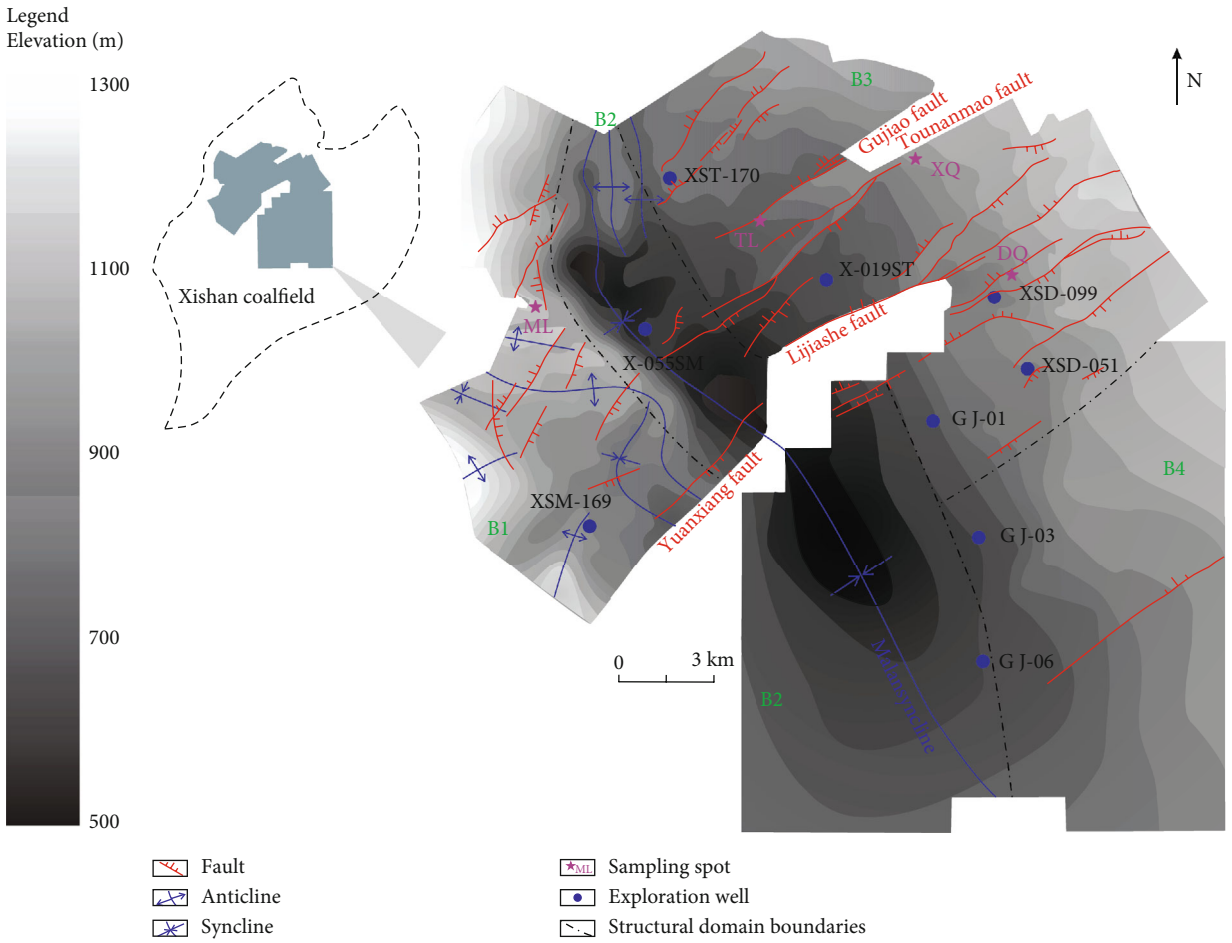

Figure 2: Geological structure and elevation of the No. 8 coal seam in Gujiao CBM field. B1–B4 are structural domains.

2. Geological Settings

The Gujiao CBM field is located in the northwest part of Xishan coalfield, including Dongqu, Tunlan, Malan, and Xingjiashe well fields (Figure 1). The structural contour map of the No. 8 coal seam is shown in Figure 2. Current tectonic structural morphology is mainly controlled by Malan syncline in this area. A series of large-scale NE-SW normal faults developed in this area such as Gujiao fault, Lijiashe fault, and Yuanxiang fault. Some small folds developed in the western region [38]. For the purpose of assessment, the Gujiao CBM field is subdivided into four structural domains (i.e., blocks B1–B4) according to the structural morphology and fracture development character (Figure 2).

Block B1 locates in the region of the Malan syncline's west limb. This block contains an east-dipping monocline with abundant small-scale folds and normal faults. Block B2 is the nucleus area of the Malan syncline. The structure of this block is relatively simple. Only a few faults and small-scale synclines are developed in the northern region. The region of the Malan syncline's eastern limb is further subdivided into two domains. Block B3 is the north part, which declines from northeast to southwest. A series of parallel large-scale northeast-southwest normal faults are developed in this area. Block B4 is the south part, whose structural characteristic is definitely inconsistent with block B3. The structure is relatively simple in this domain.

The strata preserved in the Gujiao CBM field include rocks of the Archaeozoic, Proterozoic, Cambrian, Ordovician, Pennsylvanian, Permian, Triassic, and Quaternary Systems. The main coal-bearing strata are the Benxi Formation and the Taiyuan Formation of the Pennsylvanian System and the Shanxi Formation and the Lower Shihezi Formation of the Permian System [38]. The principal targets for CBM development are coal seam No. 2 in the Shanxi Formation and Nos. 8 and 9 in the Taiyuan Formation (Figure 3), with thicknesses of 1-8 m, 1-4 m, and 1-6 m, respectively [42]. No.8 coal seam is the target in this research.

3. Method and Dataset

3.1. Sampling and Experiments. Four coal blocks were collected in the study area (Figure 1). All samples were collected from fresh coal mining face in underground coal mines. In order to minimize the influence of tectonic deformation and macroscopic coal type on the experimental results, the primary structural semibright coal samples were selected for experiment. These samples were treated to 60-80 mesh (0.18-0.25 mm). After moisture-equilibrium treatment, isothermal adsorption experiments were carried out at 25, 30,

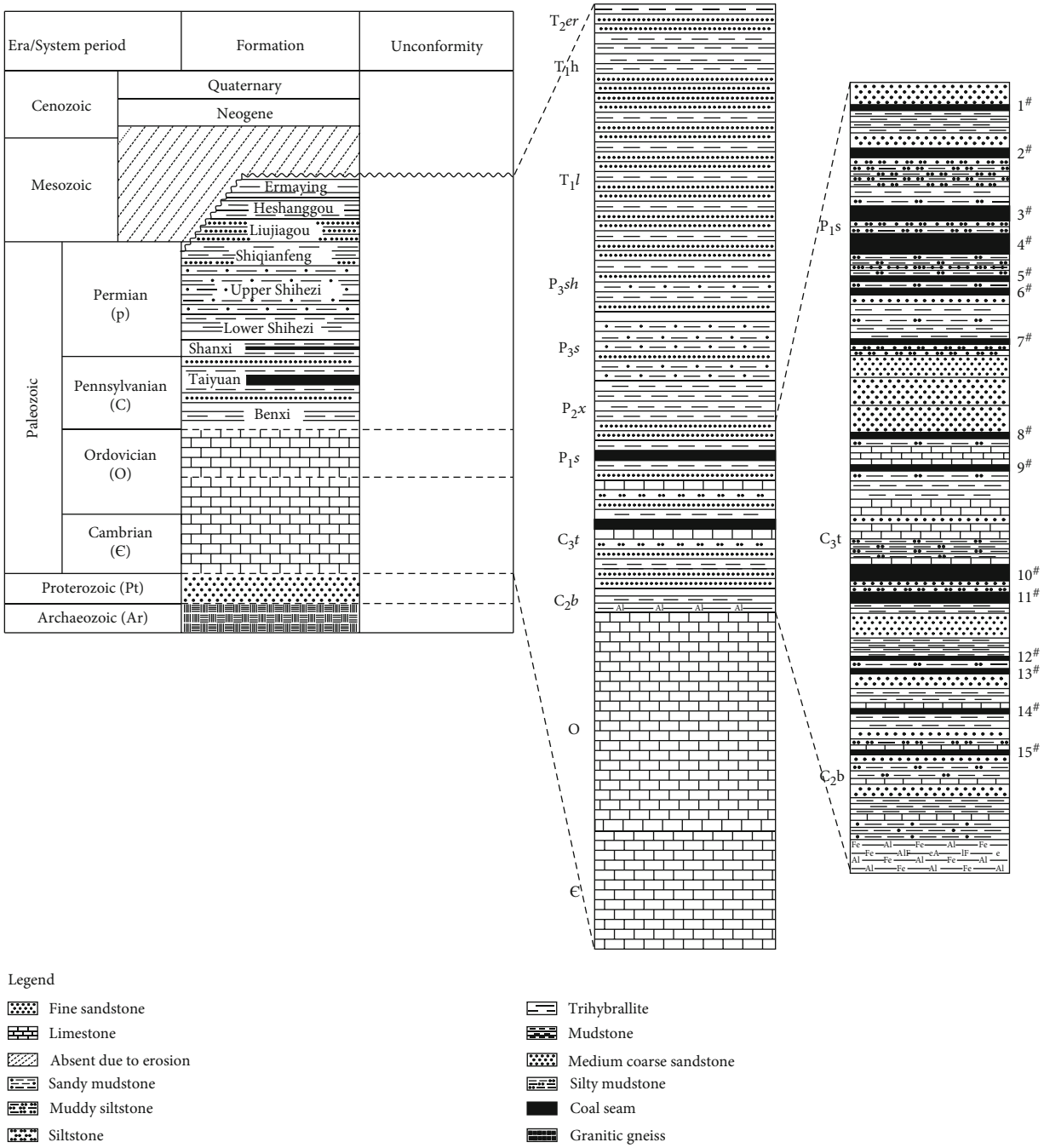

Figure 3: Stratigraphic column of the Gujiao CBM field. The dashed lines indicate the formation unconformity boundary.

40, 50, 60, and 70°C under an equilibrium pressure of up to 20 MPa. Combining with the simulated results of coal reservoir condition (pressure and temperature) evolution, these isotherms were used to characterize the adsorption capacity evolution character of coal reservoir during an uplifting process.

3.2. Simulation Process. Data of 9 exploration wells were used to simulate the evolution of reservoir formation (Figure 2). The data of proximate analysis, coal seam burial depth, thickness, vitrinite reflectance, gas content, and others were used for simulation research. Table 1 provides an example of the input database of the XST-019 well.

The dynamic equilibrium model proposed by Wei et al. [53, 54] was used to simulate the geological evolution history in this study. The tectonic subsidence history, geothermal field evolution history, and methane generation features were simulated by using a commercial computer software program PetroMod 2012. More details can be found in our previous work [45].

4. Results and Discussion

4.1. The Evolution History of Xishan Coalfield. As a part of Xishan coalfield, the geological evolution histories (the

Table 1: The database of simulation nodes that contain well XST-019.

Parameter	Value	Parameter	Value
X^a	4192416.47	Y^a	19598982.88
Recent burial depth[a] (m)	609.96	$V_L{}^a$ (m^3/t)	25.93
$P_L{}^a$ (MPa)	3.04	Reservoir pressure[a] (MPa)	7.93
Gas content in air-dry basis[a] (m^3/t)	16.46	Gas saturation[a] (%)	95.19
Moisture[a] (%)	0.65	Ash yield[a] (%)	16.87
Vitrinite[a] (%)	74.90	Inertinite[a] (%)	24.70
Liptinite[a] (%)	—	Volatile matter[a] (%)	17.14
Coal thickness[a] (m)	3.60	$R_{o,max}{}^a$ (%)	1.24
Turning point of $R_o{}^b$ (Ma)	284.87, 250, 215, 200.62	$R_{o,max}$ at turning point[b] (%)	0.37, 0.47, 0.76, 1.33
Burial depth turning point of bottom coal seam[b] (Ma)	299.7, 285.3, 250.5, 215.4, 180.2, 165.6, 144.7, 130, 64.9, 46.1, 10.6, 0	Burial depth of bottom coal seam at turning point[b] (m)	43.9, 146.9, 822.9, 3017.9, 2579.9, 2833.9, 2535.9, 2184.9, 1530.9, 1038.9, 843.9, 609.9
Turing point of geotemperature gradient[b] (Ma)	306.5, 235, 215, 200, 180, 50, 0	Geo-temperature gradient at turning point[b] (°C/100 m)	2.8, 3, 3.2, 6.46, 3.2, 3.05, 2.9

V_L and P_L are Langmuir volume (in air-dry base) and Langmuir pressure. [a]The data are obtained from wellbore, geophysical logging, and experiments (isothermal adsorption tests, maceral measurements, vitrinite reflectivity measurements, proximate analysis). [b]The data are obtained from the subsidence, geothermal, and organic maturation history simulations.

tectonic and subsidence evolution, geothermal evolution, and coal maturation history) of coal reservoir in Gujiao CBM field were strongly controlled by the evolution process of Xishan coalfield. Since the Hercynian movement, the tectonic and subsidence evolution process of Xishan coalfield can be divided into six stages, accompanied with two magmatic activities (Figure 4).

In stage I (306.1-250 Ma), affected by the Hercynian movement, the North China plate began to subside, and a series of near north-south direction coal accumulation depressions were formed in Xishan coalfield [25, 55]. Then, Pennsylvanian paralic coal-bearing rock series, Permian continental coal-bearing rock series, and continental clastic rock series were deposited continuously (Figure 4(a)).

In stage II (250-215 Ma), during the Indosinian orogeny period, the coalfield subsided rapidly and Triassic strata were deposited. The burial depth of coal-bearing strata reached the maximum [56, 57] (Figure 4(b)).

In stage III (215-180 Ma), the whole coalfield experienced tectonic uplift and sedimentary rocks suffered denudation. As a result of the Early Yanshanian orogeny, the coalfield had shown heterogeneous evolution characteristics. Affected by the continuous development of the east-west direction tectonic zone of Yangqu-Meng county in the north of Xishan coalfield, the northern part of Xishan coalfield was uplifted (Figure 4(c)) [55]. The Permo-Pennsylvanian coal seams and Ordovician limestone were exposed to the surface in this area, and the Xishan coalfield was separated with the northern Ningwu coalfield. For the southeast part, the Qixian concealed rock was developed in this stage which caused an uplift and denudation in this area (Figure 4(c)) [36].

In stage IV (180-165 Ma), the coalfield experienced tectonic subsidence. Jurassic strata were deposited in depression areas in this stage [20]. Influenced by the east-west compression force, a series of north-south direction syncline structures were formed. Malan syncline and Shuiyuguan syncline were formed initially (it is estimated that they were connected at this time). The Jiaocheng fault was also formed initially, and it was thrust nature at this time (Figure 4(d)) [58].

In stage V (165-65 Ma), during the Middle-Late Yanshanian orogeny period, influenced by the composite effects of regional east-west compressive stress, slowly uplifting of Lvliang mountain (120-65 Ma), and the development of Huyan mountain intrusion (141-125 Ma) [22], the whole coalfield experienced tectonic uplift, especially the western part of the coalfield. The direction of Malan syncline's axis changed, and the Malan syncline separated from Shuiyuguan syncline in this period (Figure 4(e)) [20].

In stage VI (65 Ma-Now), affected by the accelerated uplift of Lvliang mountain in the Himalayan orogeny period [59, 60], Xishan coalfield sustained uplift and suffered denudation. Influenced by the northwest-southeast tension stress field, a series of normal faults were formed in the coalfield [59, 61]. At this time, the Jiaocheng fault changed from thrust to normal fault [25]. Significant subsidence occurred in the area on the upper wall of the fault (Figure 4(f)). Finally, the current structural character was formed.

4.2. Tectonic and Subsidence Evolution in Gujiao CBM Field. As a part of Xishan coalfield, the evolution process of coal-bearing strata in Gujiao CBM field could also be divided into six stages, which are deposition, burial, uplift, reburial, rapid uplift, and step erosion (Figure 5).

4.2.1. Stage I: Late Pennsylvanian and Permian Periods (306.1-250 Ma). Affected by the Hercynian movement, the Gujiao CBM field began to subside, and coal-bearing strata from the Pennsylvanian to the Lower Permian Systems were deposited (Figure 4(a)) [25, 55]. During the Pennsylvanian

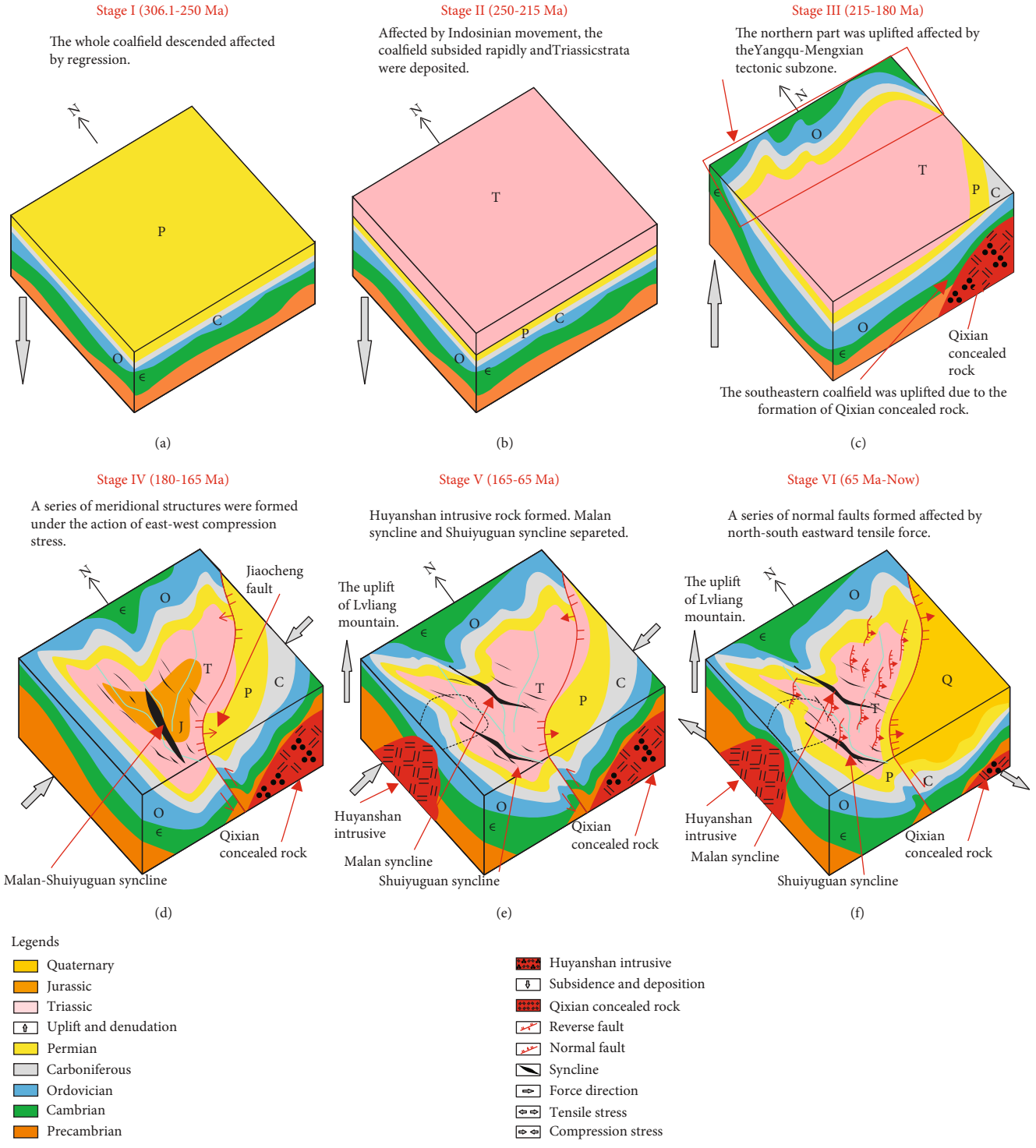

Figure 4: Schematic diagram of Xishan coalfield evolution.

Taiyuan period, the paralic sedimentary coal-bearing strata had been deposited with a deposition rate of 12.3-19.7 m/Ma and a sedimentary thickness of 92-146 m. Then, in the Permian Shanxi period, the sedimentary environment transited from paralic to continental. The deposition rate and sedimentary thickness were 2.6-3.8 m/Ma and 38-55 m, respectively. After the deposition of these Permo-Pennsylvanian coal-bearing strata, the sedimentary environment became relatively dryer in the Permian Shihezi-Shiqianfeng period. Continental variegated clastic rocks were deposited with a deposition rate of 48.3-59.8 m/Ma and a sedimentary thickness of about 654-810 m.

4.2.2. Stage II: Early and Middle Triassic Periods (250-215 Ma). Abundant river-lake face red clastic rocks were deposited in this stage with a deposition rate of 62.3-

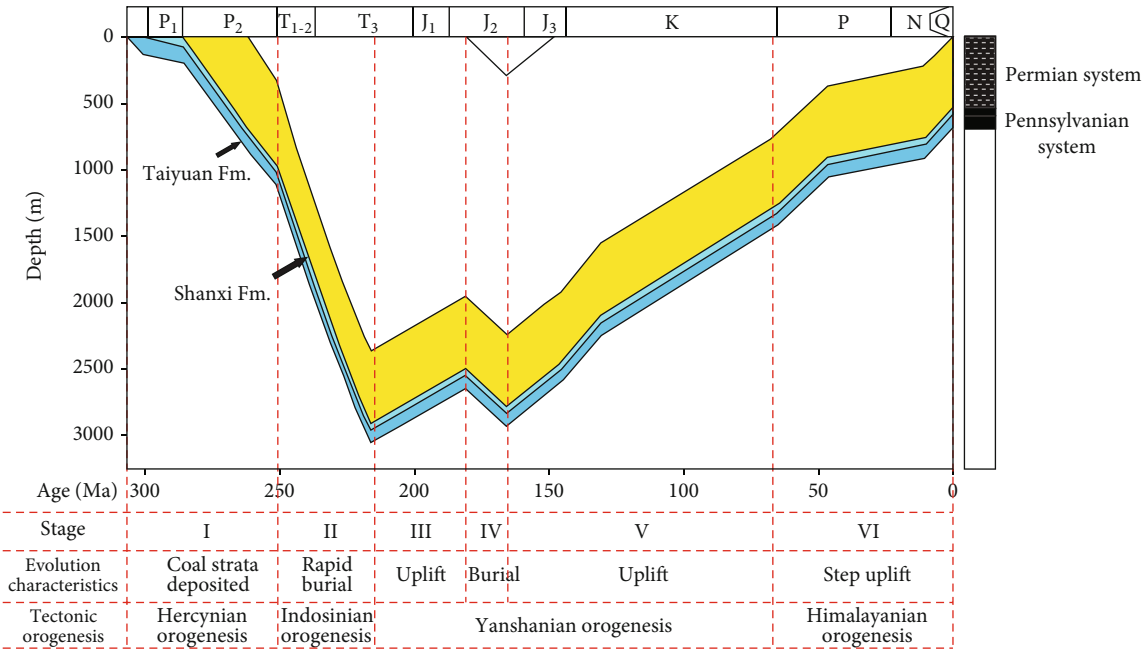

Figure 5: Typical tectonic movement and burial history curve for the coal-bearing strata in the study area.

66.6 m/Ma and a sedimentary thickness of about 2182-2332 m. The strata of the Triassic (Liujiagou Formation, the Heshanggou Formation, and the Ermaying Formation) were deposited successively in the study area [38]. The coal reservoir reached its maximum depth at the end of Middle Triassic (Figure 4(b)).

4.2.3. Stage III: Late Triassic and Early Jurassic Periods (215-180 Ma). In this stage, the study area was in a state of uplifting with a rate of 11.4-14.3 m/Ma and suffered denudation with an erosion thickness of 401-498 m. The eroded thicknesses of northern and southeast part of research area were more than elsewhere due to the development of the east-west direction tectonic zone of Yangqu-Meng county in the north and Qixian concealed rock in the southeast, respectively (Figure 4(c)) [22, 55].

4.2.4. Stage IV: Middle Jurassic Period (180-165 Ma). During the fourth stage, subsidence occurred due to the Middle Yanshanian orogeny in the North China platform. The Permo-Pennsylvanian coal-bearing strata were buried deeply again, and approximately 263-298 m of continuous sedimentary strata was deposited with a rate of 17.5-19.8 m/Ma [20].

4.2.5. Stage V: Late Jurassic Period to Late Cretaceous Period (165-65 Ma). In this stage, the Middle-Late Yanshanian Epoch, the tectonic environment of the study area changed from subsiding to uplifting. Once again, the coal-bearing strata suffered denudation with a rate of 12.1-15.6 m/Ma. Affected by the forming of Huyan mountain intrusion and uplifting of Lvliang mountain, the sedimentary rocks in the southwestern part of the study area were eroded most (Figure 4(e)) [22, 59].

4.2.6. Stage VI: Cenozoic Era (65 Ma-Now). Since the Cenozoic Era, the study area had experienced three stages of uplift [51]: first, uplifting with a rate of 20.34-31.17 m/Ma (65-46 Ma); second, uplifting with a relative slower rate of 4.29-6.58 m/Ma (46-10 Ma); and third, uplifting rapidly with a rate of 23.19-35.53 m/Ma (10 Ma- Now). The study area suffered stepped erosion, correspondingly (Figure 5) [59, 61].

4.3. Geothermal Evolution and Coal Maturation. The geothermal evolution and coal maturation characters are illustrated in Figure 6. In stage I (306.5-250 Ma), the main deposition period of the coal-bearing strata, the geothermal gradient was about 2.8°C/100 m and the coal reservoir was buried shallowly. The low temperature of coal seam led to a limited organic matter maturity (Table 2). In stage II (250-215 Ma), the study area subsided rapidly. The temperature of coal seam was increasing gradually during the long-term deposition process. At the end of Middle Triassic period, the temperature of coal seam was about 105°C when the burial depth of coal seam reached its maximum (Table 2). The vitrinite reflectance (R_o, %) of the coal seam was approximately 0.7% at that time (Figure 6). Then, in the uplifting stage (stage III), affected by the development of Qixian concealed rock (215-180 Ma) in the southeast of study area (Figure 4(c)), an abnormal geothermal field was formed (Figure 6). Due to the superposition of magma heat, the geothermal gradient in the study area increased significantly, reaching 11.84°C/100 m in some areas [22]. The regional magma thermal metamorphism led to the significant increase of coal reservoir organic maturity. The vitrinite reflectance (R_o, %) of coal seam was approximately 1.3-2.06% (Table 2), showing a decrease trend from southeast to northwest. In stage IV (180-165 Ma), the study area experienced a short-term subsidence and deposited the Jurassic strata. The geothermal field returned to normal level, and the geotemperature decreased substantially (Figure 6). Coal organic matter maturing stagnated in this stage (Table 2).

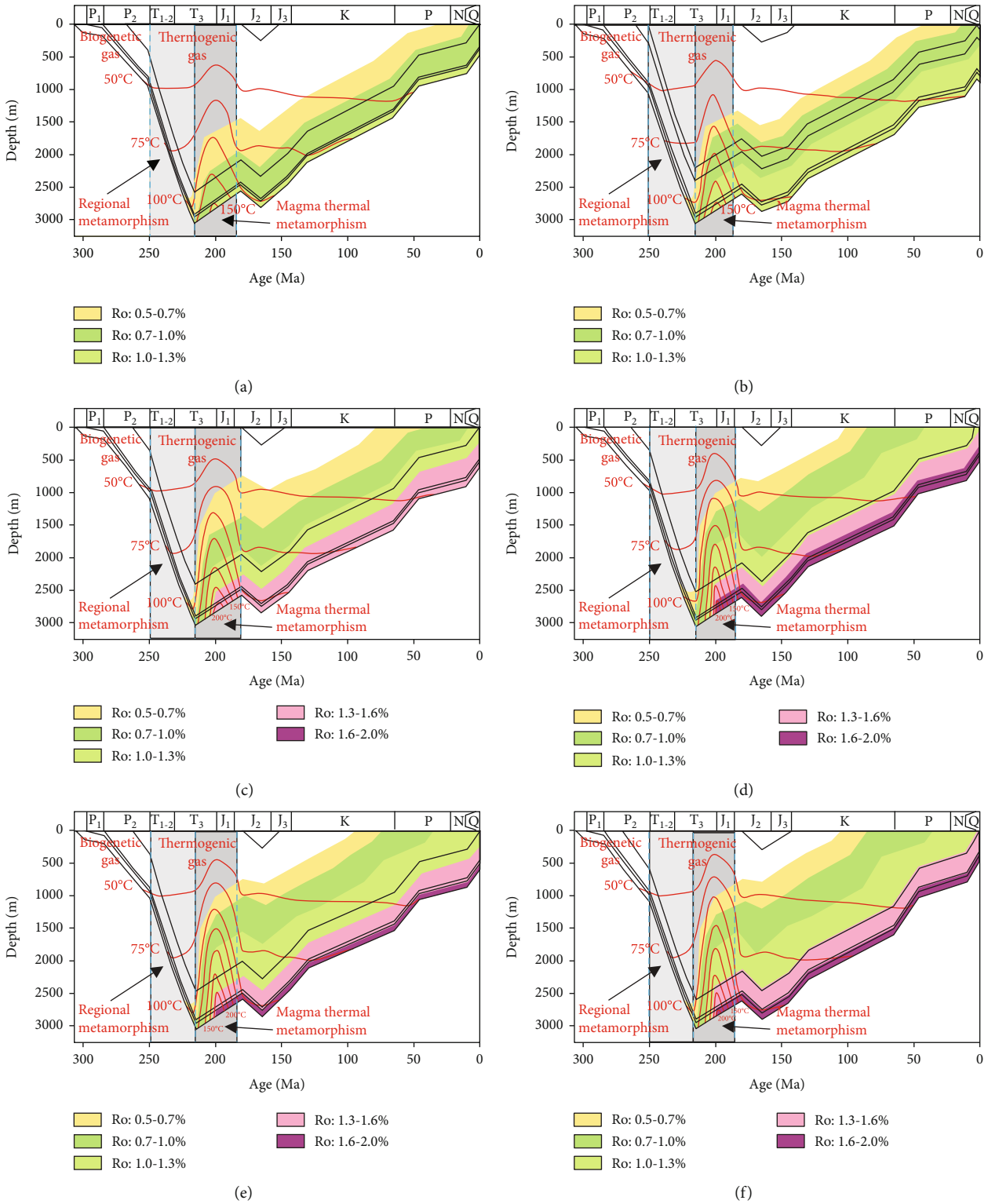

Figure 6: Continued.

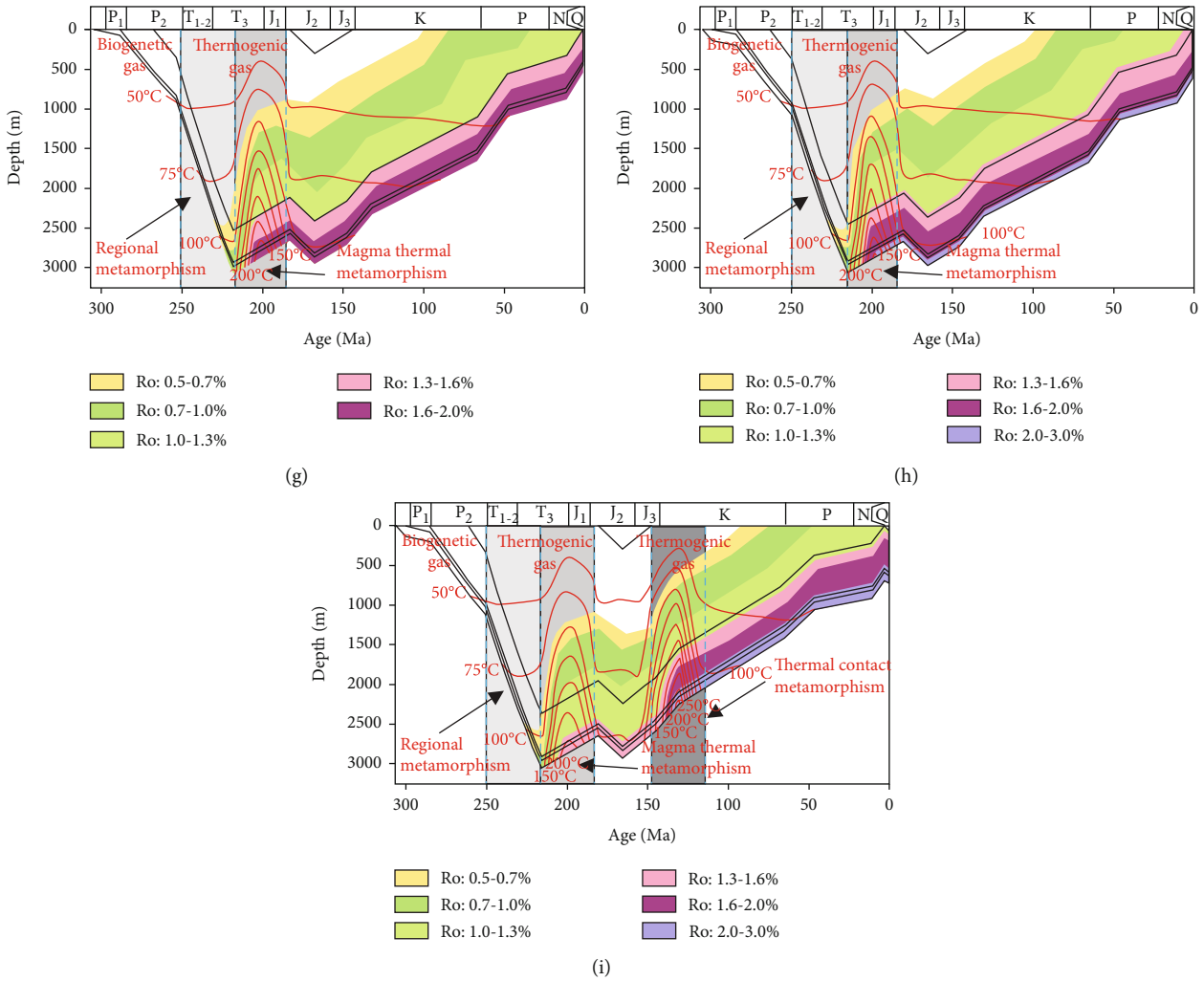

Figure 6: Temperature and maturity history curve for the coal-bearing strata of well XST-170 (a), XSM-055 (b), XST-019 (c), XSD-051 (d), XSD-099 (e), GJ-01 (f), GJ-03 (g), GJ-06 (h), and XSM-169 (i).

Then, in the next stage (stage V from 165 to 65 Ma), coal-bearing strata suffered denudation due to a long-term structural uplift. For the early period in stage V (165-141 Ma), structural uplifting led to further decreasing of coal seam temperature, and coal organic matter maturing continued to stagnate (Table 2). For the middle period in stage V (141-125 Ma), the formation of the Huyan mountain rock mass resulted in a significant increase of geothermal gradient in the western part of the Xishan coalfield (Figures 4(e) and 6(i)). The thermal contact metamorphism caused further maturation of coal organic matter (Table 2). The coal rank was distributed around the Huyan mountain in a circular belt. Within a short distance, the coal rank changed from super anthracite to high-volatile bituminous C [22]. Limited by the scale of the intrusive rock mass, only a small range of the study area was affected by this magma thermal event, which corresponds to the vicinity of the XSM-169 well in the southwest study area. For the last period in stage V (125-65 Ma) and stage VI (65 Ma-Now), the geothermal gradient reverted to a lower level gradually, the coal reservoir temperature decreased substantially, and the maturation of coal organic matter stopped (Table 2).

4.4. CBM Accumulation Process. In each evolution stage, the in situ gas content of the coal seam was mainly affected by the coal adsorption capacity and reservoir conditions (pressure and temperature) during the evolution process. An experimental simulation method modified from Bustin and Bustin [62] was used to investigate the evolutionary process of CBM accumulation in our previous work [45]. In this work, a similar experimental simulation work was also conducted. As the pressure and temperature of coal reservoir decreased, the coal adsorption capacity increased firstly and then decreased (i.e., the uplifting process) (Figure 7). Table 3 shows the adsorption capacity evolution characteristics in the domains of B1 and B3.

Combining with the results from simulation using the dynamic equilibrium model, the experimental results shown in Figure 7 and Table 3 were used to simulate the CBM accumulation processes and the formation history in the study

Table 2: The vitrinite reflectance and reservoir temperature of the coal reservoir during geothermal evolution processes.

Stage		I	II	III	IV	V			VI
						V_1	V_2	V_3	
Geological time	From	306.5	250	215	180	165	141	125	65
	To	250	215	180	165	141	125	65	Now
XST-170	R_o (%)	0.45	0.7	1.03	1.03	1.03	1.03	1.03	1.03
	T_{MAX} (°C)	38.78	104.32	207.98	105.56	94.26	83.16	60.76	43.60
XSM-169	R_o (%)	0.45	0.72	1.6	1.6	1.6	2.5	2.5	2.5
	T_{MAX} (°C)	44.01	105.77	217.71	111.00	100.44	271.32	61.24	47.29
XSM-055	R_o (%)	0.45	0.71	1.2	1.2	1.2	1.2	1.2	1.2
	T_{MAX} (°C)	41.81	104.90	212.47	108.12	103.32	91.80	69.40	53.58
XST-019	R_o (%)	0.45	0.71	1.46	1.46	1.46	1.46	1.46	1.46
	T_{MAX} (°C)	42.96	104.90	211.72	107.80	98.20	86.68	65.88	48.55
XSD-099	R_o (%)	0.45	0.71	1.72	1.72	1.72	1.72	1.72	1.72
	T_{MAX} (°C)	51.25	104.90	211.72	107.80	95.00	83.48	64.28	46.95
XSD-051	R_o (%)	0.45	0.72	1.88	1.88	1.88	1.88	1.88	1.88
	T_{MAX} (°C)	39.60	105.19	213.97	109.40	96.60	84.76	63.96	46.00
GJ-01	R_o (%)	0.45	0.72	1.83	1.83	1.83	1.83	1.83	1.83
	T_{MAX} (°C)	44.02	104.32	212.47	108.76	100.76	88.92	66.52	46.04
GJ-03	R_o (%)	0.45	0.73	1.93	1.93	1.93	1.93	1.93	1.93
	T_{MAX} (°C)	39.73	104.90	215.46	110.36	102.36	90.36	67.96	48.11
GJ-06	R_o (%)	0.45	0.74	2.06	2.06	2.06	2.06	2.06	2.06
	T_{MAX} (°C)	42.65	105.19	217.71	111.64	103.64	91.48	69.08	49.56

T_{MAX} is the maximum temperature of coal reservoir in each geothermal evolution stage.

area. The output of the simulation includes burial depth; cumulative gas production; cumulative gas diffusion; R_o; in situ gas content at each geological time; and gas production, diffusion, and retention features during each geological evolutionary stage. Table 4 provides two examples of the simulation results for simulation nodes that contain well XSM-169 and XST-019, which represent that the coal reservoir experienced three-stage and two-stage thermal metamorphism processes, respectively. The evolution of the CBM reservoir of the No. 8 coal is shown in Figure 8. Consisting with the tectonic evolution history (Figure 4) and thermal evolution history (Figure 6), the entire CBM reservoir formation evolution can also be divided into six stages (Figure 8 and Table 4).

In the first stage (306.5-250 Ma), the shallowly buried-immature stage, biogenerating gas was the main products in this low-temperature reservoir condition. However, the biogenic gas was almost dissipated due to the shallow depth and absence of an effective local reservoir cap. In the second stage (250-215 Ma), the deeply buried stage, the coal seam had undergone deep metamorphism process, accompanied with the generation of primary plutonic metamorphism gases. A few amounts of this primary CBM were stored in coal seam, which was the most dissipated. In the third stage, during the Late Triassic-Early Jurassic (215-180 Ma), affected by the concealed rock mass in Qixian County, an abnormal geothermal field was formed which made the coal organic matter maturated rapidly in most parts of the study area (Figure 8 and Table 4). A large amount of secondary coalbed gas generated in this stage, accompanied with strong gas diffusion. The fourth stage was the short-term deposition stage occurring between 180 and 165 Ma. As the organic matter maturation and hydrocarbon generation stagnated, only gas diffusion existed in this period. The fifth stage (165-130 Ma) was subdivided into three substages. The substage V_1 was a dissipation stage, from 165 to 141 Ma. The organic matter maturation and hydrocarbon generation continue to stagnate; only gas diffusion existed in this substage (Table 4). Then, in the substage V_2, the thermal contact metamorphism caused further maturation of coal organic matter in the southwest part of research area (e.g., well XSM-169), whereas the gas further diffused in the other areas (e.g., well XST-019) as shown in Figure 8 and Table 4. In the southwestern part, the generation of third coalbed gas led to strong gas diffusion (Table 4). For the substage V_3 (125-65 Ma) and stage VI (65 Ma-Now), affected by the Late Yanshanian orogeny and Himalayan orogeny, the overlying strata were uplifted and eroded continuously, and more gas escaped from coal reservoir.

4.5. Hydrocarbon System Evolution and Geological Control Effects. The Gujiao CBM field contains one hydrocarbon system, as shown in Figure 9. During the histories of hydrocarbon generation, expulsion, and migration processes, there are three major hydrocarbon generation and accumulation periods, i.e., the Indosinian, the Early Yanshanian, and the Middle Yanshanian, respectively. The Permo-Pennsylvanian coal seams are the source rocks of gas in this hydrocarbon system. The Late Permian strata are seal rocks

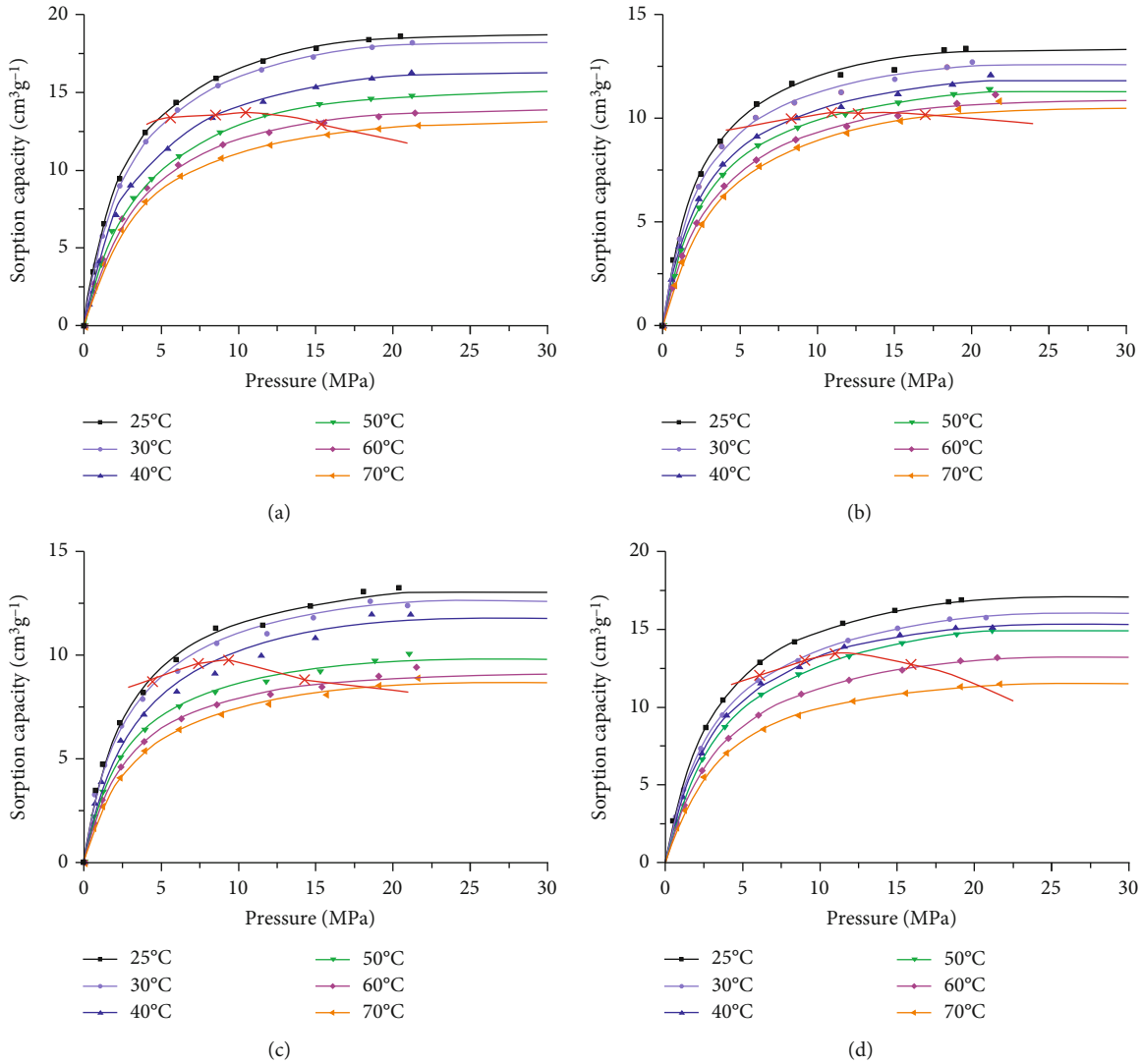

Figure 7: The methane adsorption capacity at different temperatures and pressures. Four samples DQ (a), ML (b), TL (c), and XQ (d) are from the domains of B1 (sample b) and B3 (samples a–d), respectively. The sorption capacities curve (red line) was plotted at the pressure and temperature conditions from reservoir subsidence and geothermal field history (the pressure gradient was set as 1.0 MPa/100 m).

that prevent gas diffusion. Hydrogeological conditions and tectonic structures had different effects on hydrocarbon migration and preservation. Four critical tectonic events have had a significant impact on gas production, accumulation, and diffusion (Figure 9).

Coal-bearing strata were deposited in the Late Pennsylvania and Early Permian periods (stage I) during which the primary biogenic methane was produced and almost dissipated (Figure 8). After this shallowly buried period, the generation, expulsion, and accumulation processes of CBM were affected by the following episodic tectonic movements.

During stage II, the Early-Middle Triassic Indosinian orogeny was the first critical tectonic event that affected the generation of primary CBM (Figure 9). The maturity of coal increased with the increase of depth from the edge of the basin to the center (i.e., from north to south). Gas content at the end of this stage and gas diffusion during this stage were 6.2-7.4 m^3/t and 11.2-13 m^3/t, respectively (Figure 10). The distribution of gas content was consistent with the distribution characteristic of coal organic vitrinite reflectance (Table 2). The deeper buried coal seams had a higher paleotemperature, accompanied with a higher organic maturity. The higher organic maturity led to a higher gas production capacity and gas diffusion (Figure 10). The retention and dissipation of primary gases were controlled by the amount of gas produced and the sealing conditions of the coal reservoir.

The second critical tectonic event was the Early Yanshanian orogeny (Stage III in Figures 5 and 9). In this stage, the development of the Late Triassic-Early Jurassic Qixian concealed rock mass led to an abnormal geothermal field, which accelerated the maturation process of coal organic matter. The reservoir temperature decreased gradually from southeast to northwest (Table 2). Hydrocarbon generation and dissipation in most parts of the study area reached their maximum values over the entire geological evolution history. The maturity of coal organic matter increased significantly, reaching a maximum of 2.06% (well GJ-06) in the southeast part of study area. The gas production was about 28.12-

Table 3: The sorption capacity, gas content, and saturation evolution characteristics of the sampling sites after thermal metamorphism processes.

Structural domain	Sample	Age (Ma)	0	10	46	65.5	125
		Depth (m)	829.68	1090.78	1264.84	1700.00	2346.15
		Q_S (cm^3/g)	5.25	9.05	10.06	11.58	14.74
B1	ML	P (MPa)	8.30	10.91	12.65	17.00	23.46
		Q_C (cm^3/g)	9.93	10.23	10.18	10.13	9.74
		S (%)	52.85	88.45	98.81	114.36	151.35
		Depth (m)	555.08	850.56	1047.54	1540.00	2093.85
		Q_S (cm^3/g)	12.22	16.82	18.24	20.59	25.82
	DQ	P (MPa)	5.55	8.51	10.48	15.40	20.94
		Q_C (cm^3/g)	13.33	13.54	13.70	12.93	11.73
		S (%)	91.65	124.24	133.16	159.23	220.20
		Depth (m)	445.45	740.82	937.73	1430.00	2076.15
		Q_S (cm^3/g)	5.50	6.54	7.19	8.10	9.73
B3	TL	P (MPa)	4.45	7.41	9.38	14.30	20.76
		Q_C (cm^3/g)	8.67	9.55	9.71	8.77	8.20
		S (%)	63.43	68.48	74.07	92.40	118.71
		Depth (m)	610.00	904.00	1100.00	1590.00	2190.00
		Q_S (cm^3/g)	12.10	14.64	16.22	18.44	22.41
	XQ	P (MPa)	6.10	9.04	11.00	15.90	21.90
		Q_C (cm^3/g)	12.07	13.03	13.48	12.76	10.70
		S (%)	100.22	112.32	120.34	144.52	209.40

Q_S and P are the gas content and reservoir pressure obtained from the simulations of CBM reservoir accumulation history. Q_C is the sorption capacity obtained from the adsorption capacity evolution simulation. S is the gas saturation of the sampling sites.

Table 4: The simulation results of the simulation nodes that contain well XSM-169 and XST-019.

	Stage	I	II	III	IV	V			VI		
						V_1	V_2	V_3	VI_1	VI_2	VI_3
Geological time	From	306.5	250	215	180	165	141	125	65	46	10
	To	250	215	180	165	141	125	65	46	10	Now
	R_o (%)	0.45	0.72	1.6	1.6	1.6	2.5	2.5	2.5	2.5	2.5
	Reservoir temperature (°C)	44.01	105.77	217.71	111.00	100.44	271.32	61.24	47.29	41.21	34.49
	Cumulative gas production (m^3/t)	2.78	18.88	107.71	107.71	107.71	209.10	209.10	209.10	209.10	209.10
XSM-169	Gas production in each stage (m^3/t)	2.78	16.11	88.83	0	0	101.39	0	0	0	0
	Gas diffusion in each stage (m^3/t)	1.94	10.16	47.81	14.34	5.38	90.63	16.15	4.84	3.23	8.07
	Cumulative gas diffusion (m^3/t)	1.94	12.10	59.91	74.25	79.63	170.26	186.41	191.25	194.48	202.55
	Gas content (m^3/t)	0.83	6.78	47.80	33.46	28.08	38.84	22.70	17.85	14.62	6.55
	R_o (%)	0.45	0.71	1.46	1.46	1.46	1.46	1.46	1.46	1.46	1.46
	Reservoir temperature (°C)	42.96	104.90	211.72	107.80	98.20	86.68	65.88	48.55	41.22	32.69
	Cumulative gas production (m^3/t)	2.78	18.15	91.54	91.54	91.54	91.54	91.54	91.54	91.54	91.54
XST-019	Gas production in each stage (m^3/t)	2.78	15.38	74.39	0	0	0	0	0	0	0
	Gas diffusion in each stage (m^3/t)	1.94	9.73	39.94	11.97	3.17	2.38	3.96	2.22	1.59	2.54
	Cumulative gas diffusion (m^3/t)	1.94	11.67	51.61	63.58	66.75	69.13	73.09	75.31	76.9	79.44
	Gas content (m^3/t)	0.83	6.48	39.93	27.96	24.78	22.41	18.44	16.22	14.64	12.1

Well XSM-169 and XST-019 represent that the coal reservoir had experienced three-stage and two-stage thermal metamorphism processes, respectively.

140.97 m^3/t in this stage, showing a downward trend from southeast to northwest. The amount of gas diffusion was determined by the gas generation characteristics. Gas content at the end of this stage and gas diffusion during this stage were 17.2-59.4 m^3/t and 17.2-89 m^3/t, respectively (Figure 11). The distributions of vitrinite reflectance, gas

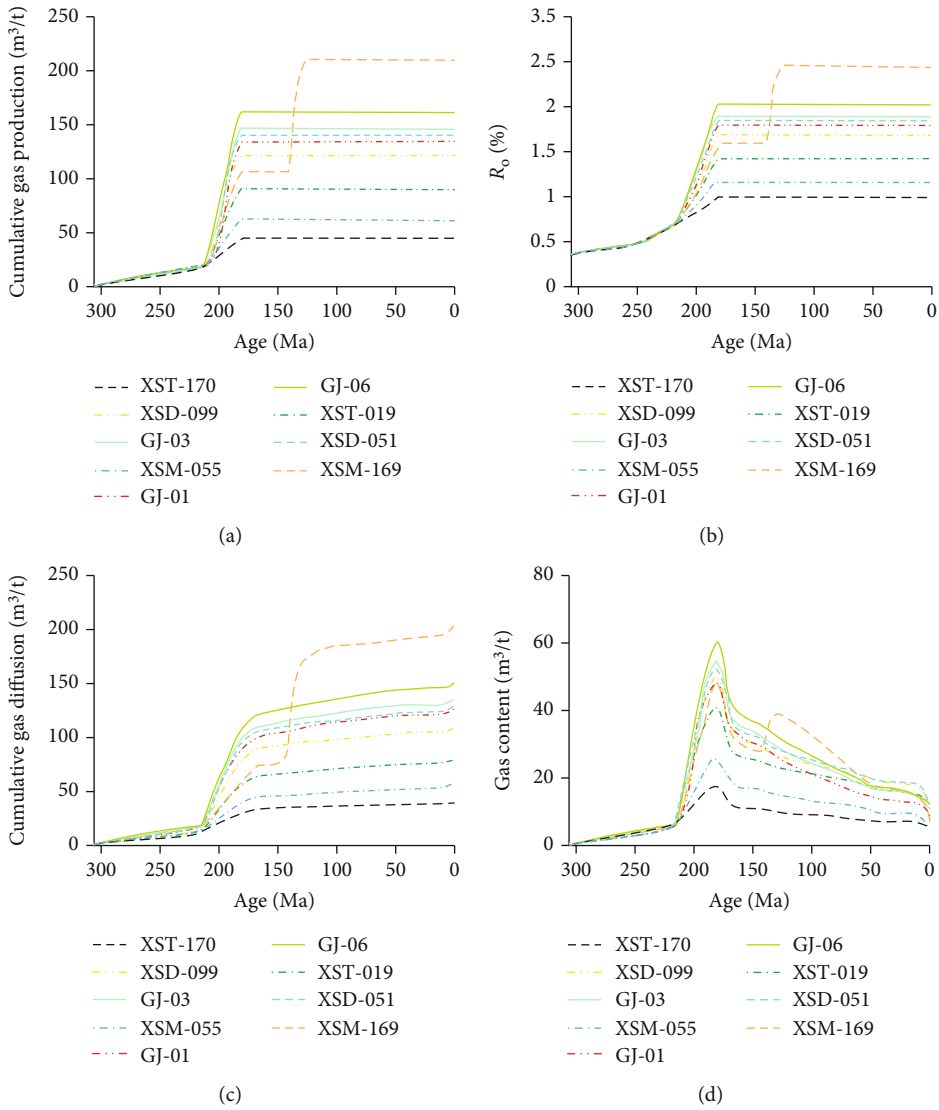

Figure 8: Curves show the CBM reservoir formation evolution history: (a) cumulative gas generation; (b) coal organic maturity; (c) cumulative gas diffusion; (d) gas content.

content, and gas diffusion were similar to the distribution of paleotemperature (Figure 11 and Table 2). The second critical tectonic event controlled the paleotemperature field variation which resulted in the high gas content in B4 and the south area of B2.

During the following period of 185-145 Ma (stages IV and V_1 in Table 4), the study area was deposited briefly and then uplifted. Due to the low temperature of coal reservoir, hydrocarbon generation stagnated, and only gas diffusion existed in this period. Gas content at the end of this stage and gas diffusion during this stage were 10.7-35.6 m^3/t and 6.5-23.8 m^3/t, respectively (Figure 12). The amount of gas diffusion was high in the southeast (B4 and the south area of B2 domain), which inherited the gas content distribution characteristic at the previous stage (Figures 11(a) and 12(b)). This result implies that the methane concentration was a much more important factor than others for gas diffusion in this stage.

After this gas diffusion period, the third critical tectonic event occurred in the Middle Yanshanian orogeny (145-130 Ma: stage V_2 in Table 4) (i.e., the formation of the Huyan mountain rock mass). Due to the intrusion of Huyan mountain rock mass, an abnormal geothermal field was formed in the southwest part of study area and the coal seams in there experienced their third hydrocarbon-generation process. The reservoir temperature was distributed in a ring band and decreased from the southwest corner to the northeast in southwest research area (south area of B1 and southwest of B2). Hydrocarbon generation and gas diffusion showed the same trend that decreased from the southwest to the northeast (Figure 12(b)). The coal rank reached 2.5% in the area of well XSM-169, and the volume of gas production was 101.4 m^3/t in this area during this stage. As for the other areas, due to the further decrease of temperature, the hydrocarbon generation stopped and the gas in coal seams further escaped. In these low-paleotemperature field areas, the gas diffusion was dominated by the in situ hydrocarbon

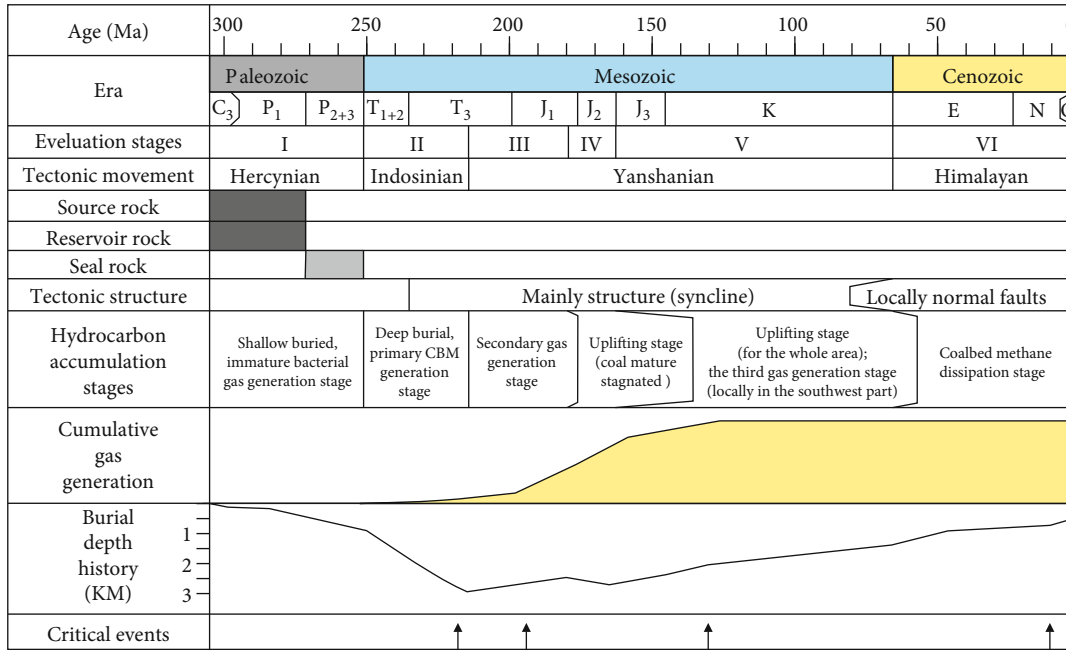

FIGURE 9: Extended essential element diagram showing the hydrocarbon system present in the study area with relation to tectonic activity and general tectonic behavior.

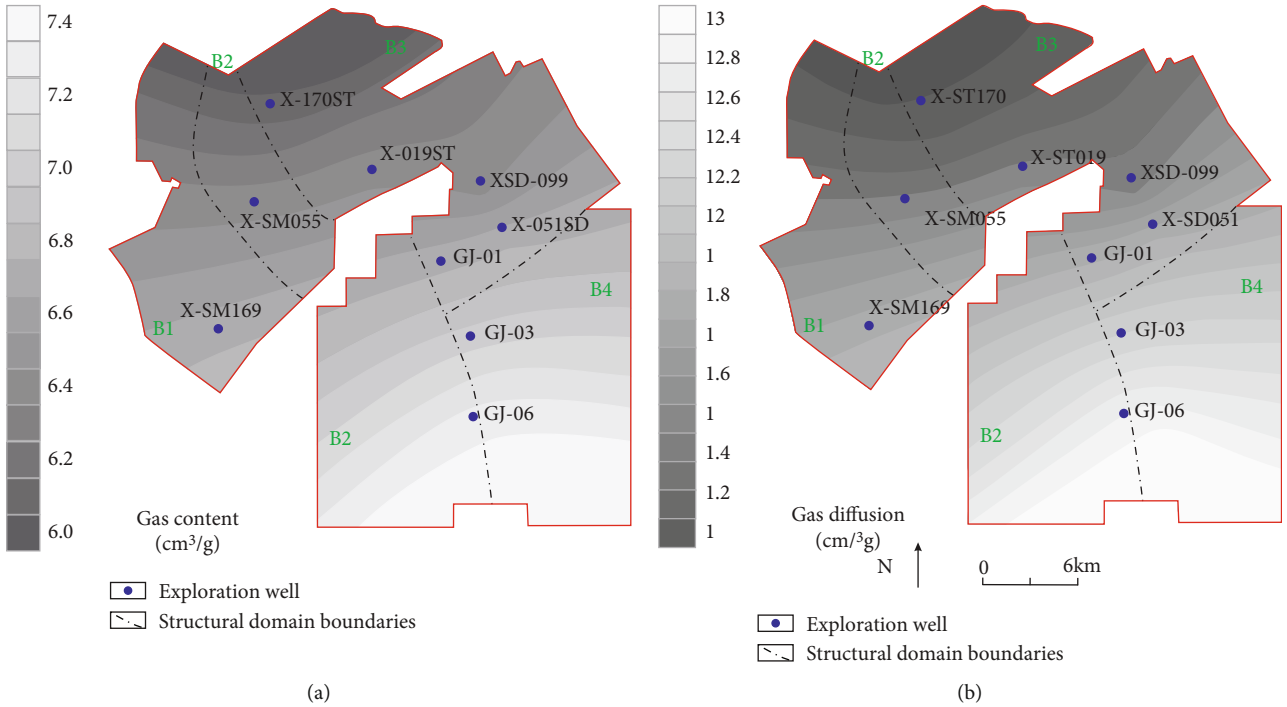

FIGURE 10: Distribution characteristics of gas content (a) at the end of Middle Triassic period and gas diffusion during the Indosinian orogeny (b).

concentration. The gas content at the end of the previous evolution period (Figure 12(a)) controlled the variation of gas accumulation and dissipation in these low temperature areas. Gas content at the end of this stage and gas diffusion during this stage were 9.7-38.8 m^3/t and 1-90.6 m^3/t, respectively (Figure 13). The gas content and gas diffusion reached their maximum value in the southwest region and decreased radially to the northeast, whereas in the areas unaffected by Huyan mountain rock mass, the hydrocarbon variation characteristics of the previous period were inherited.

In substage V_3, influenced by the uplifting of Lvliang mountain in this period and the intrusion of Huyan mountain rock mass in the former period, the west to southwest part of the study area uplifted more than elsewhere

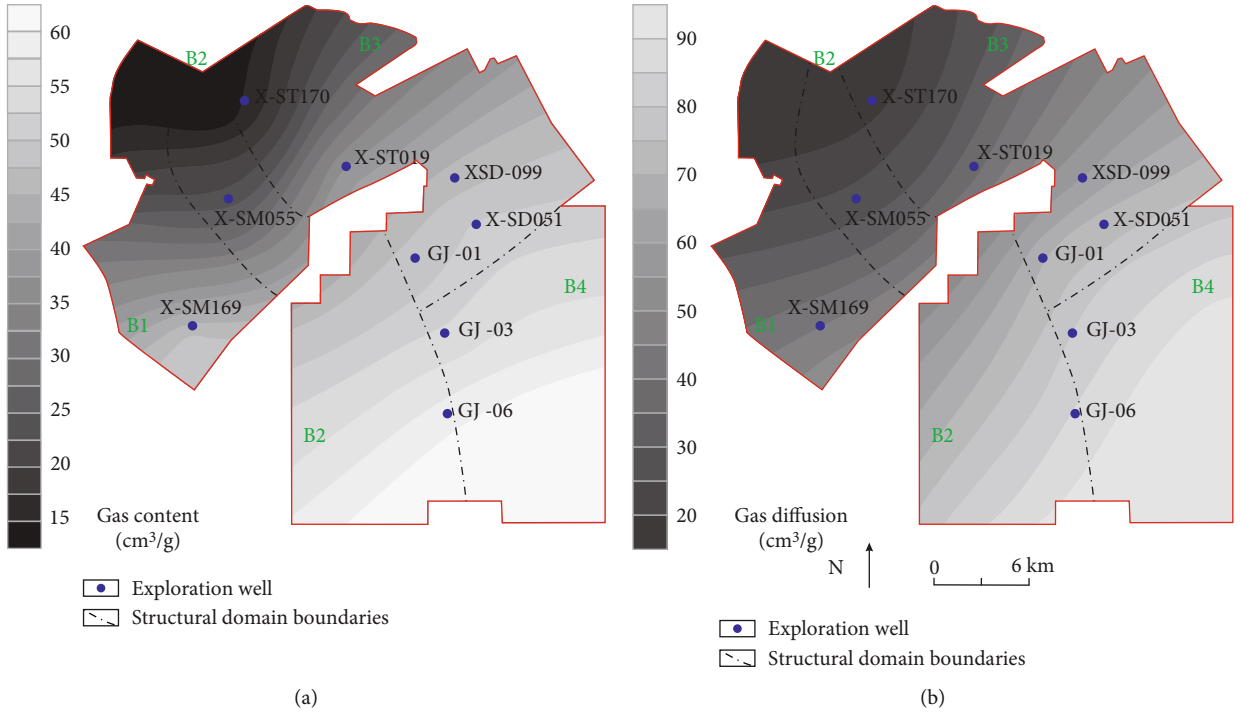

Figure 11: Distribution characteristics of gas content (a) at the end of Early Jurassic period and gas diffusion during the Early Yanshanian orogeny (b).

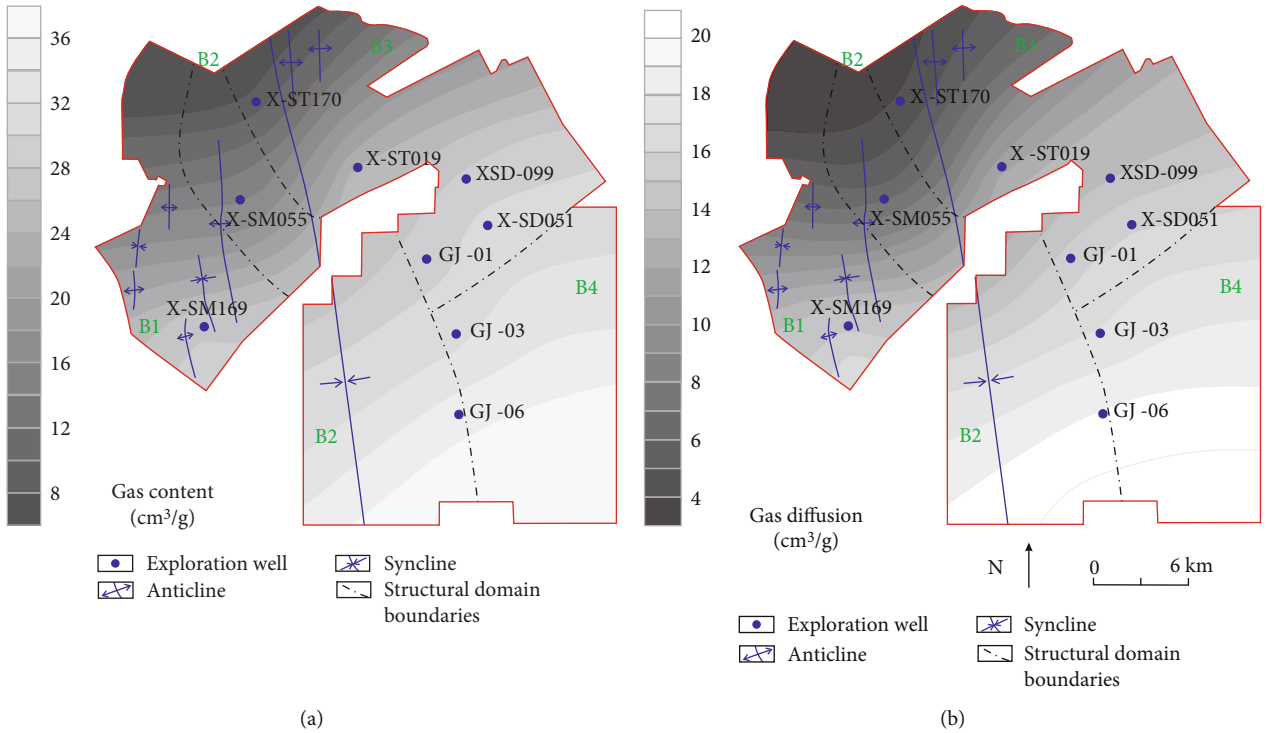

Figure 12: Distribution characteristics of gas content (a) at the end of the substage V_1 and gas diffusion during the stage IV and substage V_1 (b).

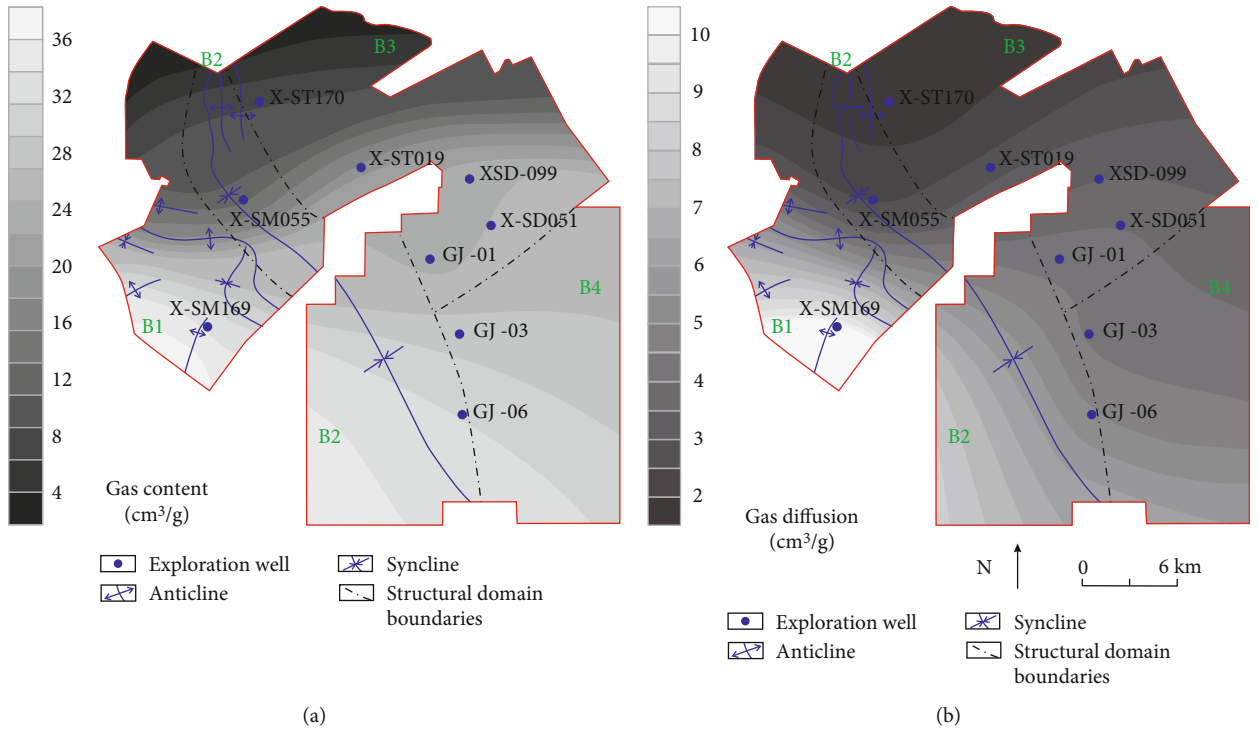

Figure 13: Distribution characteristics of gas content (a) at the end of the substage V_2 and gas diffusion during this stage (b).

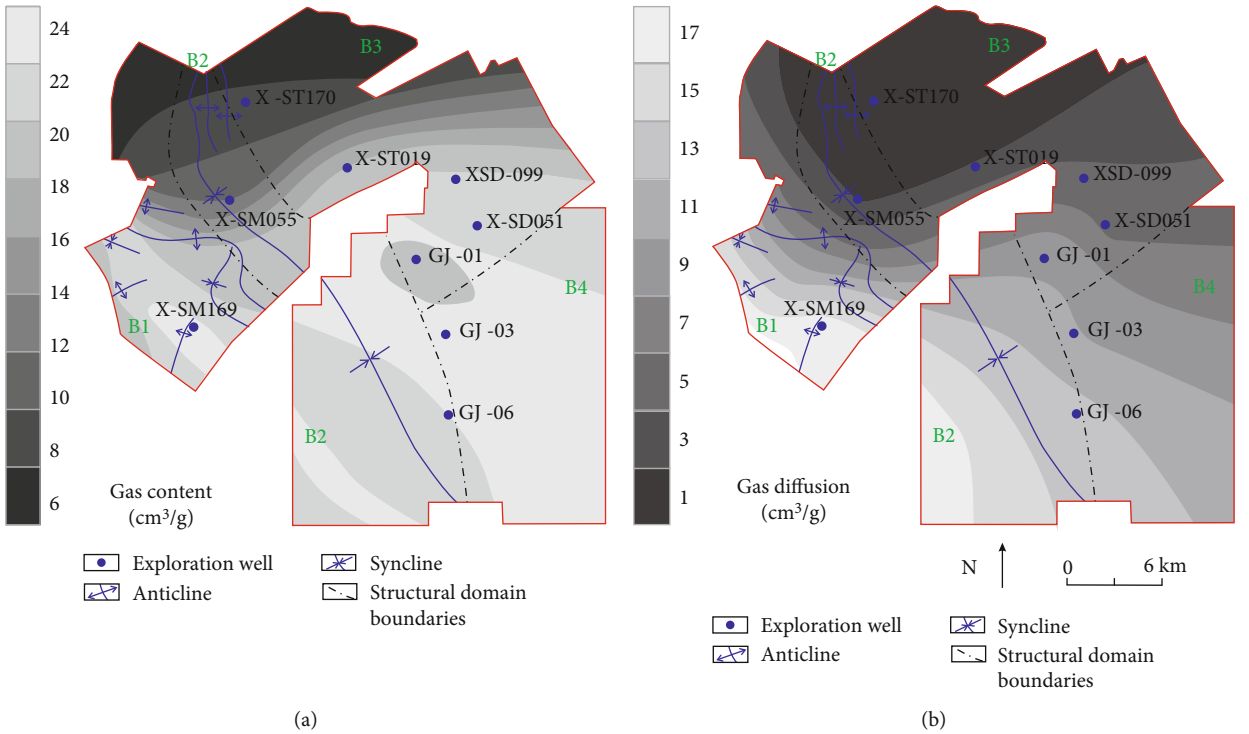

Figure 14: Distribution characteristics of gas content (a) at the end of Cretaceous and gas diffusion during substage V_3 (b).

accompanied with a higher gas escape degree. The amount of gas diffusion was 1.6-16.2 m^3/t, showing a decrease trend from southwest to northeast (Figure 14(b)). At the end of the stage, the gas content was 8.1-22.7 m^3/t, as shown in Figure 14(a).

Since the Cenozoic Era, the study area has experienced three stages of uplift [51]. During the first and second uplifting stages (substage VI_1 and VI_2), under the influence of the Early and Middle Himalayan tectonic movement, the study area was uplifted in a stepped manner. The gas diffusion

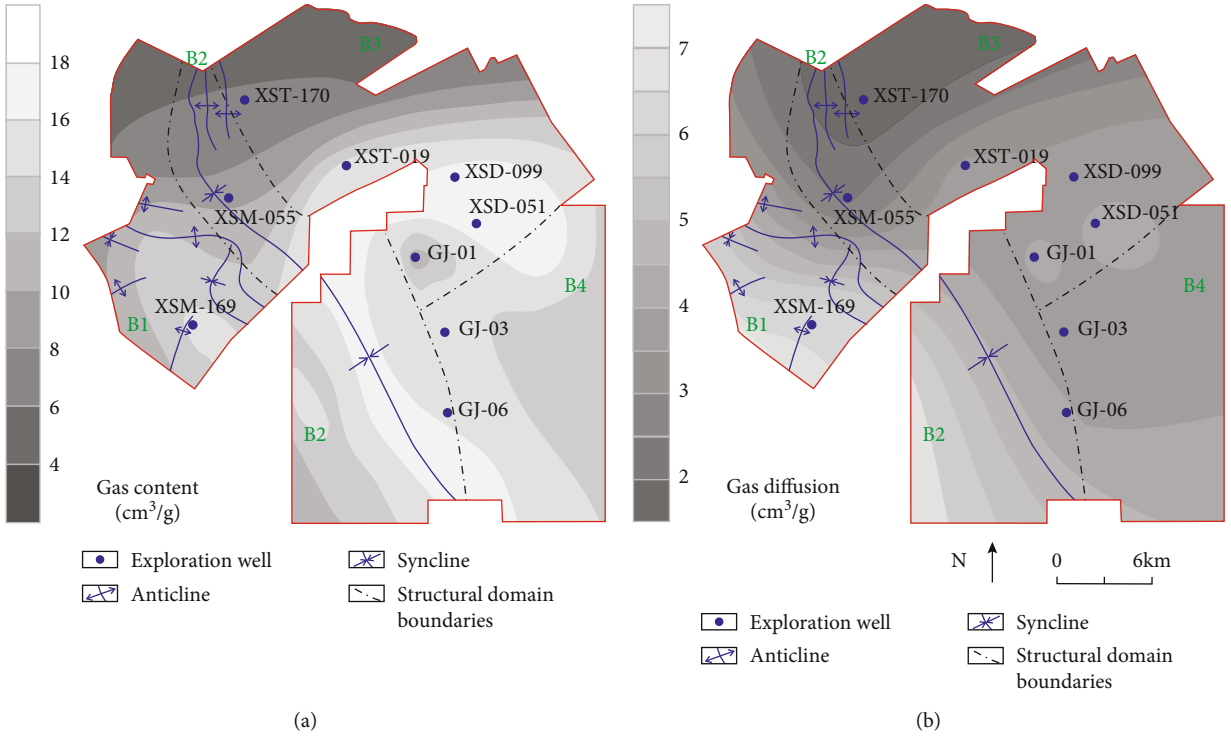

FIGURE 15: Distribution characteristics of gas content (a) at the end of substage VI_2 and gas diffusion during substage VI_1 and VI_2 (b).

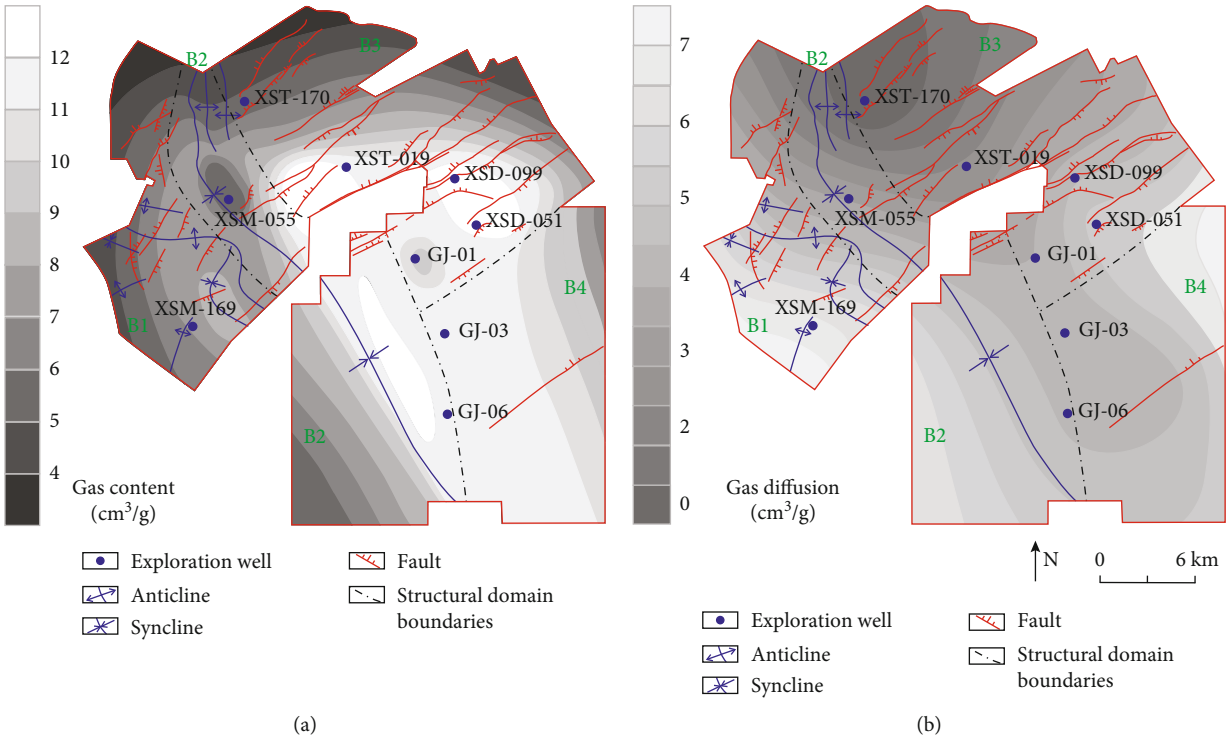

FIGURE 16: Distribution characteristics of current gas content (a) and gas diffusion during substage VI_3 (b).

was dominated by the hydrocarbon concentration at the end of the previous stage (Figures 14(a) and 15(b)). After this evolution period, the gas content was about 6.5-17.4 m^3/t (Figure 15(a)), and its distribution characteristics were roughly consistent with the distribution characteristics at the previous stage (Figure 14(a)). The gas saturation was

relatively low in the west part of study area (B1 domain and north of B2 domain) due to sustaining uplifting of Lvliang mountain in the west (Table 3).

The fourth critical tectonic event occurred in the Late Himalayan period (substage VI_3). During this stage, the study area experienced a sharp uplift. In this period, the development of the Fenhe graben caused the structural inversion in the northeast to eastern regions of the study area [59]. The stress field transformed from the squeezed state to the stretched state. Affected by the northwest-southeast tension stress, a series of northeast-southwest normal faults were formed, mainly in the northeastern part of the study area. The development of these extensional structures resulted in strong gas diffusion (Figure 16). The gas saturation and gas content decreased rapidly in the northeast part of the study area (east part of B3 domain) (Table 3 and Figure 16). Moreover, during this stage, the limestone areas in the northwest and north part of the coalfield were the main recharge runoff area of the study area. The groundwater flowed from these recharge areas to the low-lying zone of the study area. The gas was carried to the axis area of syncline for accumulation [16, 26].

In general, the combining effects of basin uplifting, tectonic inversion (the formation of extensional faults), and hydrogeological characteristics controlled the gas content and dissipation characteristics of reservoirs in this evolution period.

5. Conclusion

The evolution of coalbed methane reservoir can be subdivided into six evolutionary stages: (1) shallowly buried, immature stage; (2) deeply buried, primary coalbed methane accumulation stage; (3) concealed rock mass influenced secondary gas generation stage; (4) low temperature, maturation stagnated stage, (5) uplifting, locally third gas generation stage; and (6) sustaining uplifting and structural inversion, further coalbed methane dissipation stage.

The formation, preservation, and dissipation of coalbed methane were mainly affected by four critical tectonic events. The first critical tectonic event during the Indosinian period of the Early-Middle Triassic controlled the first hydrocarbon generation process in the study area. The second critical tectonic event in the Early Yanshanian period, Qixian concealed rock mass magma-heat event, affected the distribution of secondary gas generation distribution characteristic and resulted in higher gas generation in southeast part of research area. The third critical tectonic event in the Middle Yanshanian period, Huyan mountain intrusive rock mass magma-heat event, dominated local third gas generation distribution characteristic and resulted in higher gas generation in the southwest research area (south area of B1 and southwest of B2). The fourth critical event, i.e., the Late Himalayan tectonic inversion, caused the further diffusion of gas and reduced the gas content and saturation in coal reservoir, especially in the northeast part of study area (east part of B3 domain). The combination of these four critical tectonic events led to the high gas heterogeneity distribution of coalbed methane reservoirs in Gujiao coalbed methane field, Xishan coalfield.

Data Availability

All data are derived from my experimental results, which can be provided in the appendix of the paper if necessary.

Conflicts of Interest

The authors declare that they have no conflicts of interest.

Acknowledgments

This research was funded by the National Natural Science Foundation of China (41902178, 41973077, U1910204); Open Fund of Beijing Key Laboratory of Unconventional Natural Gas Geological Evaluation and Development Engineering, China University of Geosciences (Beijing) (2019BJ02001); the Natural Science Foundation of Shanxi Province, China (201701D221026); and Research project of China United Coalbed Methane Co., Ltd (ZZGSSAYJ-PYTH2020-300).

References

[1] Y. Yang, W. Li, and L. Ma, "Tectonic and stratigraphic controls of hydrocarbon systems in the Ordos basin: a multicycle cratonic basin in central China," *American Association of Petroleum Geologists Bulletin*, vol. 89, no. 2, pp. 255–269, 2005.

[2] C. B. Che, H. L. Yang, F. B. Li et al., "Exploration and development prospects of coal bed methane (CBM) resources in China," *China Mining Magazine*, vol. 17, pp. 1–4, 2008.

[3] Y. Cai, D. Liu, Y. Yao, J. Li, and Y. Qiu, "Geological controls on prediction of coalbed methane of No. 3 coal seam in Southern Qinshui Basin, North China," *International Journal of Coal Geology*, vol. 88, no. 2-3, pp. 101–112, 2011.

[4] Z. P. Meng, J. C. Zhang, and R. Wang, "In-situ stress, pore pressure and stress-dependent permeability in the southern Qinshui Basin," *International Journal of Rock Mechanics and Mining Sciences*, vol. 48, pp. 122–131, 2020.

[5] H. Guo, R. Liu, Z. Yu et al., "Pyrosequencing reveals the dominance of methylotrophic methanogenesis in a coal bed methane reservoir associated with Eastern Ordos Basin in China," *International Journal of Coal Geology*, vol. 93, pp. 56–61, 2012.

[6] Y. Lv, D. Tang, H. Xu, and H. Luo, "Production characteristics and the key factors in high-rank coalbed methane fields: a case study on the Fanzhuang Block, southern Qinshui Basin, China," *International Journal of Coal Geology*, vol. 96-97, pp. 93–108, 2012.

[7] C. N. Zou, Z. Yang, S. Z. Tao et al., "Continuous hydrocarbon accumulation over a large area as a distinguishing characteristic of unconventional petroleum: the Ordos Basin, North-Central China," *Earth-Science Reviews*, vol. 126, pp. 358–369, 2013.

[8] S. Tao, D. Tang, H. Xu, L. Gao, and Y. Fang, "Factors controlling high-yield coalbed methane vertical wells in the Fanzhuang Block, Southern Qinshui Basin," *International Journal of Coal Geology*, vol. 134-135, pp. 38–45, 2014.

[9] Z. Li, D. Liu, P. G. Ranjith, Y. Cai, and Y. Wang, "Geological controls on variable gas concentrations: a case study of the

northern Gujiao Block, northwestern Qinshui Basin, China," *Marine and Petroleum Geology*, vol. 92, pp. 582–596, 2018.

[10] K. Aminian and S. Ameri, "Predicting production performance of CBM reservoirs," *Journal of Natural Gas Science and Engineering*, vol. 1, no. 1-2, pp. 25–30, 2009.

[11] J. Chen, Z. Wang, Y. Yang, A. W. Xianhua, C. Yanpeng, and Z. Qingbo, "Influencing factors on coal-bed methane production of single well: a case of Fanzhuang Block in the south part of Qinshui Basin," *Acta Petrolei Sinica*, vol. 30, no. 3, pp. 409–416, 2009.

[12] H. L. Liu, H. Y. Wang, G. L. Zhao, G. Z. Li, Y. Fan, and H. J. Liu, "The influence of the Yanshanian tectonic thermal event on the high-yield and enrichment of coalbed methane in Xishan, Taiyuan," *Natural Gas Industry*, vol. 25, no. 1, pp. 29–32, 2005.

[13] Z. H. Zhang, "Analysis on the present situation and prospect of CBM exploration and development in Gujiao," *World Nonferrous Metals*, vol. 7, pp. 95-96, 2017.

[14] P. Xia, F. G. Zeng, and X. X. Song, "Geologic structural controls on coalbed methane content of the no. 8 coal seam, Gujiao area, Shanxi, China," *Applied Ecology and Environmental Research*, vol. 15, no. 1, pp. 51–68, 2017.

[15] J. J. Bian, P. Xia, J. Wang et al., "Evaluation of coal-bed methane reservoir in Gujiao mining area of Xishan coal field," *Coal Technology*, vol. 36, no. 60, pp. 67-68, 2017.

[16] P. Xia, F. G. Zeng, and X. X. Song, "Evaluation on distribution mode and development effect of coalbed methane in Gujiao mining area of Xishan coalfield," *Coal Science and Technology*, vol. 41, no. 7, pp. 245–254, 2019.

[17] Y. C. Duan, "Application of stable isotopes in the study of Taishan Xishan coalfield," *Coal Geology and Exploration*, vol. 3, pp. 15–18, 1988.

[18] S. J. Wang, B. L. Tian, and Y. T. Guo, "Palaeocommunity and its succession of peat swamp of no. 7 seam in Xishan coalfield," *Journal of China Coal Society*, vol. 1, pp. 88–92, 1995.

[19] A. M. Fang, G. J. Lei, K. L. Jin, J. X. Lu, and Q. L. Hou, "An anthracographic study on no. 7 coal in Xishan coalfield, Shanxi," *China Coalfield Geology*, vol. 15, pp. 12–16, 2003.

[20] J. G. Zhao, *The Morphology of Collapse Pillar Forest in Coal Measure and Structure-Hydrology Evolution in Xishan Coalfield*, Taiyuan University of Technology, Taiyuan, China, 2004.

[21] W. J. Zhao, W. M. Cai, and A. M. Fang, "A study on genetic type of No. 7 coal seam in Xishan coalfield, Shanxi Province," *Coal Geology of China*, vol. 6, pp. 29–32, 2007.

[22] B. L. Sun, F. G. Zeng, X. Li, and C. Liu, "Time of coal rank formation for Ximing-Duerping mining area in Xishan coalfield, Taiyuan: evidence from zircon fission track dating," *Journal of China Coal Society*, vol. 11, pp. 2023–2029, 2013.

[23] J. Wang, L. J. Chen, W. D. Wu, H. U. Liang, B. Z. Zhang, and J. D. Liao, "Geochemical characteristics and geological significance of trace elements in Xishan coalfield, Taiyuan," *Science Technology and Engineering*, vol. 16, no. 15, pp. 15–21, 2016.

[24] G. Wang, Y. Xie, Y. Qin et al., "Element geochemical characteristics and formation environment for the roof, floor and gangue of coal seams in the Gujiao mining area, Xishan coalfield, China," *Journal of Geochemical Exploration*, vol. 190, pp. 336–344, 2018.

[25] B. B. Han, *Porosity and Permeability of Coal Reservoirs in Xishan Gujiao Mining Area and Prediction of Favorable Construction Areas*, China University of Mining and Technology, 2015.

[26] Y. R. Zhu, B. L. Sun, F. G. Zeng, P. Xia, P. Zhang, and Y. J. You, "Hydrogeological characteristics of CBM reservoirs and their controlling effects in Gujiao mining area, Xishan coalfield," *Journal of China Coal Society*, vol. 43, no. 3, pp. 759–769, 2018.

[27] N. Zhang, F. Zhao, P. Guo et al., "Nanoscale pore structure characterization and permeability of mudrocks and fine-grained sandstones in coal reservoirs by scanning electron microscopy, mercury intrusion porosimetry, and low-field nuclear magnetic resonance," *Geofluids*, vol. 2018, Article ID 2905141, 20 pages, 2018.

[28] L. Zeng, X. G. Sun, S. H. Cui, and J. Y. Sui, "Controlling effects of structural-hydrogeological conditions on coalbed methane accumulation in Xishan coalfield," *Coal Science and Technology*, vol. 49, no. 9, pp. 80–88, 2019.

[29] Z. Zou, D. Liu, Y. Cai, Y. Wang, and J. Li, "Geological factors and reservoir properties affecting the gas content of coal seams in the Gujiao area, northwest Qinshui basin, China," *Energies*, vol. 11, no. 5, pp. 1–21, 2018.

[30] J. B. Cheng, R. Zhou, and Y. H. Liu, "Coal petrology and quality characteristics of Shanxi Coal Forormation in Xishan coalfield," *Coal Technology*, vol. 37, no. 3, pp. 132–134, 2018.

[31] L. Wu, "Recoverable evaluation of CMB resources in Xishan mine area," *China's Coalbed Methane*, vol. 4, pp. 27–30, 2010.

[32] J. D. Pang, L. Wang, X. L. Zhang et al., "The geological conditions and resource potential analysis of coal bed gas in Gujiao area," *Science Technology and Engineering*, vol. 15, pp. 155–160, 2015.

[33] L. Wang, D. Z. Tang, H. Xu et al., "Magmatism effect on different transformation characteristics of coal reservoirs physical properties in Xishan coalfield," *Journal of China Coal Society*, vol. 8, pp. 1900–1910, 2015.

[34] B. Wang, B. Jiang, Z. B. Guo et al., "Characteristics of coalbed methane accumulation in Xishan coalfield, Qinshui basin," *Natural Gas Geoscience*, vol. 4, pp. 565–567, 2007.

[35] D. M. Liu and J. Q. Li, "Main geological controls on distribution, occurrence and enrichment patterns of coalbed methane in China," *Coal Science and Technology*, vol. 6, pp. 19–24, 2014.

[36] Q. Deng, J. D. Feng, J. W. Niu, Y. B. Zhao, and J. J. Li, "Key accumulation periods for the CBM in Xishan coalfield," *Petroleum Geology and Oilfield Development in Daqing*, vol. 6, pp. 165–170, 2015.

[37] P. Jiandong, W. Zhen, and Y. Changhua, "The control action of magmatic activity to the gas content of coal in Xishan coalfield," *Bulletin of Science and Technology*, vol. 3, pp. 29–33, 2016.

[38] G. Wang, Y. Qin, Y. W. Xie, J. Shen, and B. Huang, "Geochemical characteristics and its origin of CBM in Gujiao blocks," *Journal of China Coal Society*, vol. 41, no. 5, pp. 1180–1187, 2016.

[39] Z. Rui, Y. Yanbin, L. Dameng, C. Yidong, and W. Yingjin, "Gas potential distribution and controlling factor of coal reservoir in Taiyuan Xishan coalfield," *Coal Science and Technology*, vol. 45, no. 2, pp. 122–129, 2017.

[40] L. Zhao, Y. Qin, C. Cai et al., "Control of coal facies to adsorption-desorption divergence of coals: a case from the Xiqu Drainage Area, Gujiao CBM Block, North China," *International Journal of Coal Geology*, vol. 171, pp. 169–184, 2017.

[41] Y. H. Liu, D. N. Liu, S. L. Chang et al., "Single factor analysis of CBM reservoir forming geology in Gujiao block of Taiyuan Xishan coalfield," *China Coal*, vol. 43, no. 4, pp. 38–42, 2017.

[42] G. Wang, Y. Qin, Y. Xie et al., "Coalbed methane system potential evaluation and favourable area prediction of Gujiao blocks, Xishan coalfield, based on multi-level fuzzy mathematical analysis," *Journal of Petroleum Science and Engineering*, vol. 160, pp. 136–151, 2018.

[43] K. Zhang, Q. Liu, K. Jin, L. Wang, Y. Cheng, and Q. Tu, "Influence of overlying caprock on coalbed methane migration in the Xutuan Coal Mine, Huaibei coalfield, China: a conceptional analysis on caprock sealability," *Geofluids*, vol. 2019, Article ID 9874168, 17 pages, 2019.

[44] J. Tang, Y. Xu, G. Wang et al., "Methane in soil gas and its migration to the atmosphere in the Dawanqi oilfield, Tarim Basin, China," *Geofluids*, vol. 2019, Article ID 1693746, 10 pages, 2019.

[45] T. Yan, Y. Yao, and D. Liu, "Critical tectonic events and their geological controls on gas generation, migration, and accumulation in the Weibei coalbed methane field, southeast Ordos basin," *Journal of Natural Gas Science and Engineering*, vol. 27, pp. 1367–1380, 2015.

[46] D. F. Payne and P. J. Ortoleva, "A model for lignin alteration–part II: numerical model of natural gas generation and application to the Piceance Basin, Western Colorado," *Organic Geochemistry*, vol. 32, no. 9, pp. 1087–1101, 2001.

[47] R. C. Johnson and R. M. Flores, "Developmental geology of coalbed methane from shallow to deep in Rocky Mountain basins and in Cook Inlet-Matanuska basin, Alaska, U.S.A. and Canada," *International Journal of Coal Geology*, vol. 35, no. 1-4, pp. 241–282, 1998.

[48] C. J. Boreham, S. D. Golding, and M. Glikson, "Factors controlling the origin of gas in Australian Bowen Basin coals," *Organic Geochemistry*, vol. 29, no. 1-3, pp. 347–362, 1998.

[49] M. Faiz, A. Saghafi, N. Sherwood, and I. Wang, "The influence of petrological properties and burial history on coal seam methane reservoir characterisation, Sydney Basin, Australia," *International Journal of Coal Geology*, vol. 70, no. 1-3, pp. 193–208, 2007.

[50] R. F. Sachsenhofer, V. A. Privalov, and E. A. Panova, "Basin evolution and coal geology of the Donets Basin (Ukraine, Russia): an overview," *International Journal of Coal Geology*, vol. 89, pp. 26–40, 2012.

[51] A. Hildenbrand, B. M. Krooss, A. Busch, and R. Gaschnitz, "Evolution of methane sorption capacity of coal seams as a function of burial history – a case study from the Campine Basin, NE Belgium," *International Journal of Coal Geology*, vol. 66, no. 3, pp. 179–203, 2006.

[52] D. Alsaab, M. Elie, A. Izart et al., "Distribution of thermogenic methane in carboniferous coal seams of the Donets Basin (Ukraine): "applications to exploitation of methane and forecast of mining hazards"," *International Journal of Coal Geology*, vol. 78, no. 1, pp. 27–37, 2009.

[53] C. Wei, Y. Qin, G. G. X. Wang, X. Fu, B. Jiang, and Z. Zhang, "Simulation study on evolution of coalbed methane reservoir in Qinshui basin, China," *International Journal of Coal Geology*, vol. 72, no. 1, pp. 53–69, 2007.

[54] C. Wei, Y. Qin, G. G. X. Wang, X. Fu, and Z. Zhang, "Numerical simulation of coalbed methane generation, dissipation and retention in SE edge of Ordos Basin, China," *International Journal of Coal Geology*, vol. 82, no. 3-4, pp. 147–159, 2010.

[55] J. H. Fu, "Development mechanism and influence analysis of Xishan coalfield geologic structure," *Shanxi Coking Coal Science and Technology*, vol. 6, pp. 17–19, 2008.

[56] C.-F. Wu, Y. Qin, X.-H. Fu, and A. Y. Zeng, "Microcosmic dynamical energies of coalbed gas reservoir formation of Qinshui Basin, Shanxi Province," *Geoscience*, vol. 19, no. 3, pp. 449–457, 2005.

[57] Y. Qin, B. Jiang, J. Y. Wang et al., "Coupling control of tectonic dynamical conditions to coalbed methane reservoir formation in the Qinshui Basin, Shanxi, China," *Acta Geologica Sinica*, vol. 82, no. 10, pp. 1355–1362, 2008.

[58] Shanxi Province Geology and Mining Bureau, *Regional Geology of Shanxi Province*, geology press, Beijing, 1989.

[59] J. X. Li, L. P. Yue, C. Y. Liu, X. Y. Wang, and G. F. Li, "The tectonic-sedimentary evolution of the Lvliang mountains since the Miocene," *Journal of Stratigraphy*, vol. 31, no. 1, pp. 93–100, 2013.

[60] J. Sun, X. Zhu, and Z. Li, "Fe isotope geochemistry of hydrothermal Fe exhalites," *Acta Geologica Sinica - English Edition*, vol. 91, Supplement 1, pp. 43–54, 2017.

[61] Q. R. Zheng, *The Characteristics of Continental Crustal Evolution of North-Central Shanxi*, Taiyuan University of Technology, Taiyuan, China, 2012.

[62] A. M. M. Bustin and R. M. Bustin, "Coal reservoir saturation: impact of temperature and pressure," *AAPG Bulletin*, vol. 92, no. 1, pp. 77–86, 2008.